On the formation and transformation of Fe(III)-containing chukanovite, FeII2-xFeIIIx(OH)2-xOxCO3

J. Duboscq, M. Abdelmoula, C. Rémazeilles, M. Jeannin, R. Sabot, Ph Refait

▶ **To cite this version:**

J. Duboscq, M. Abdelmoula, C. Rémazeilles, M. Jeannin, R. Sabot, et al.. On the formation and transformation of Fe(III)-containing chukanovite, FeII2-xFeIIIx(OH)2-xOxCO3. Journal of Physics and Chemistry of Solids, 2020, 138, pp.109310. 10.1016/j.jpcs.2019.109310 . hal-02480974

HAL Id: hal-02480974

https://univ-rochelle.hal.science/hal-02480974v1

Submitted on 21 Dec 2021

HAL is a multi-disciplinary open access archive for the deposit and dissemination of scientific research documents, whether they are published or not. The documents may come from teaching and research institutions in France or abroad, or from public or private research centers.

L'archive ouverte pluridisciplinaire **HAL**, est destinée au dépôt et à la diffusion de documents scientifiques de niveau recherche, publiés ou non, émanant des établissements d'enseignement et de recherche français ou étrangers, des laboratoires publics ou privés.

Distributed under a Creative Commons Attribution - NonCommercial 4.0 International License

Version of Record: https://www.sciencedirect.com/science/article/pii/S0022369719316713
Manuscript_351708916c7308da4f878a240cfac7be

On the formation and transformation of Fe(III)-containing chukanovite, $Fe^{II}_{2-x}Fe^{III}_{x}(OH)_{2-x}O_xCO_3$

J. Duboscq[1], M. Abdelmoula[2], C. Rémazeilles[1], M. Jeannin[1], R. Sabot[1] and Ph. Refait[1,*]

[1] *Laboratoire des Sciences de l'Ingénieur pour l'Environnement (LaSIE), UMR 7356 CNRS - Université de La Rochelle, Bât. Marie Curie, Av. Michel Crépeau, 17042 La Rochelle cedex 01, France.*

[2] *Laboratoire de Chimie Physique et Microbiologie pour les Matériaux et l'Environnement (LCPME), UMR 7564 CNRS – Université de Lorraine, 405, rue de Vandoeuvre, 54600 Villers-lès-Nancy, France*

Abstract. Aqueous suspensions of Fe(II)-chukanovite were obtained by mixing $FeSO_4$ and (Na_2CO_3 + NaOH) solutions and studied by X-ray diffraction, vibrational spectroscopy (Raman and infrared) and Mössbauer spectroscopy. After 1 week of ageing in suspension in anoxic conditions, the Fe(II)-chukanovite particles remained poorly crystallized. A partial oxidation by air led to the formation of Fe(III)-containing chukanovite, i.e. $Fe^{II}_{2-x}Fe^{III}_{x}(OH)_{2-x}O_xCO_3$, with a Fe(III) proportion about 11-13%. The lattice parameters of the monoclinic structure varied with the Fe(III) content, in particular the *b* parameter decreased significantly with increasing oxidation time. Fe(III)-containing chukanovite proved metastable in anoxic conditions and transformed upon ageing at room temperature into a mixture of Fe(II)-chukanovite and magnetite Fe_3O_4. Finally, trying to form Fe(III)-containing chukanovite by co-precipitation from Fe(II) and Fe(III) dissolved species led to a mixture of Fe(II)-chukanovite, i.e. $Fe^{II}_2(OH)_2CO_3$, and sulfated green rust.

Keywords: Iron, Carbonate, X-ray diffraction, Mössbauer spectroscopy, Raman spectroscopy, Infrared spectroscopy.

* Corresponding author: Tel: +33 5 46 45 82 27; fax: +33 5 46 45 82 41

E-mail: prefait@univ-lr.fr (Ph. Refait).

© 2019 published by Elsevier. This manuscript is made available under the CC BY NC user license
https://creativecommons.org/licenses/by-nc/4.0/

1. Introduction

Chukanovite, the Fe(II) hydroxycarbonate with formula $Fe_2(OH)_2CO_3$, was reported first as a corrosion product of steel and identified as a "basic ferrous carbonate" [1]. It was discovered thirty years later as a mineral on an iron meteorite found in Russia near the city of Dronino [2] and found a common corrosion product on ferrous archaeological artifacts [3-5]. Following these discoveries, various studies were devoted to chukanovite dealing with its synthesis in laboratory conditions [6], the determination of its standard Gibbs free energy [7-9], the refinement of its crystal structure [2,10], or the understanding of its oxidation and transformation mechanisms [11,12]. Chukanovite was also observed as a corrosion product of steel in the specific conditions associated with the storage of high-level radioactive waste in deep geological disposals [10,13-16]. It might play a role on the behavior of the corrosion system, depending on the protective efficiency it can give to the corrosion product layer (CPL). In some cases, chukanovite was observed in the inner stratum of the CPL, in contact with the metal [3-5,16], or separated from the metal surface by a thin layer of conductive iron compounds such as magnetite or mackinawite [13,15,17]. If this inner stratum of chukanovite were conductive it could facilitate, in aerated conditions, the reduction of dissolved O_2 because O_2 molecules from the surrounding environment could be reduced at the outer surface of the chukanovite stratum, thus only having to diffuse through the outer part of the CPL. Chukanovite proved also a major corrosion product of permeable reactive barrier (PRB) systems [8,18-20], an environmental technology utilizing granular zero-valent iron for treating contaminated ground water. It can then affect the long-term performance of these systems.

Chukanovite may also be present as a mineral in natural environments (soils or sediments). It was reported as a product of the transformation of unstable cation-excess magnetite biogenerated by iron reducing bacteria and considered as a possible overlooked mineral phase in anoxic sediments [21]. In hydromorphic soils, it could result from the

spontaneous transformation of carbonated green rust (i.e. the mineral fougèrite [22]) in anoxic conditions [23]. In sediments, it could crystallize from a nanocrystalline hydrated Fe-carbonate precursor [24].

Chukanovite may be deficient in cations, with a consequent partial substitution of OH^- ions by H_2O, thus leading to the formula $Fe_{2-x}(OH)_{2-x}CO_3.xH_2O$ [2]. Chemical analysis of chukanovite as a corrosion product revealed that it could contain Fe(III) [1]. The composition $Fe^{II}_{1.8}Fe^{III}_{0.2}(OH)_{2.2}CO_3$ was proposed but it could not be excluded that this composition actually corresponded to that of a mixture of Fe(II)-chukanovite (i.e. $Fe^{II}_2(OH)_2CO_3$) with an amorphous FeOOH phase [1]. More recently, the formation of such Fe(III)-containing chukanovite was also assumed, but not demonstrated, and it was proposed [11] that this partially oxidized chukanovite was an intermediate transient compound during the oxidation of chukanovite to Fe(III) oxyhydroxides. The general formula $Fe^{II}_{2-x}Fe^{III}_x(OH)_{2-x}O_xCO_3$ was forwarded [11] for Fe(III)-containing chukanovite, assuming that the oxidation of a Fe^{2+} cation into a Fe^{3+} cation was accompanied by the deprotonation of an OH^- ion, i.e. the formation of an O^{2-} ion. Using hydrogen peroxide as a strong oxidizing agent, the Fe(III) oxycarbonate $Fe^{III}_2O_2CO_3$ could be obtained from chukanovite, supporting the deprotonation model [11].

In magnetite (Fe_3O_4) at room temperature, the electrons associated with the Fe(II) and Fe(III) cations present in the octahedral sites of the inverse spinel structure are delocalized and migrate within the structure thus giving magnetite its well-known electrical conductivity. Similarly, it cannot be excluded that the presence of Fe(III) in chukanovite could give this compound some electrical conductive properties. In this case, Fe(III)-containing chukanovite could play a significant role in the corrosion product layers. It could act as cathode and promote galvanic effects and corrosion cells, as observed for magnetite [25-30]. In the environment, Fe(III)-containing chukanovite would then be characterized by an in situ redox

flexibility similar to that of fougèrite [31], allowing Fe(III) to be reduced and Fe(II) to be oxidized in-situ in the crystal structure of chukanovite.

Though some previous works mention its possible formation [1,11,12], not a single study has been devoted to Fe(III)-containing chukanovite. Actually, the conditions favoring its formation and the corresponding mechanisms are not known. Besides, its stability over time is yet to be established. Actually, it was shown that Fe(II)-chukanovite was metastable with respect to siderite [9], which implies that it could transform spontaneously to siderite. The objectives of the present study were then:

- to investigate different pathways for the formation of aqueous suspensions of Fe(III)-containing chukanovite,

- to characterize Fe(III)-containing chukanovite using complementary analytical tools, namely X-ray diffraction, Raman spectroscopy, Mössbauer spectroscopy and infrared spectroscopy,

- to follow the possible transformation over time of Fe(III)-containing chukanovite in anoxic conditions.

2. Materials

All the chemical products used for the preparation of the various precipitates had a 98% min. purity.

2.1. Synthesis of Fe(II)-chukanovite suspensions

The procedure used here was derived from previous studies [6,9,11,12]. It consisted in mixing $FeSO_4 \cdot 7H_2O$, NaOH, and $Na_2CO_3 \cdot 10H_2O$ solutions with concentrations corresponding to the ratios $[FeSO_4 \cdot 7H_2O]/[NaOH] = 1.0$ and $[Na_2CO_3 \cdot 10H_2O]/[NaOH] = 0.5$. These ratios correspond to the stoichiometry of the precipitation reaction of $Fe_2(OH)_2CO_3$:

$$2Fe^{2+} + 2OH^- + CO_3^{2-} \rightarrow Fe_2(OH)_2CO_3 \quad (1)$$

All the experiments were performed with a NaOH concentration equal to 0.2 mol L^{-1}. The $FeSO_4 \cdot 7H_2O$ and $Na_2CO_3 \cdot 10H_2O$ concentrations were then equal to 0.2 mol L^{-1} and 0.1 mol L^{-1}, respectively. The volume of solution was 300 mL in each case, corresponding to a total of 0.06 mol of Fe(II). The proportion of dissolved Fe(II) species remaining in solution in equilibrium with the solid phase can be considered as negligible due to the low solubility of chukanovite in these experimental conditions [9].

Because this work was focused on Fe(III)-containing chukanovite, the reference precipitate, used as the starting point for all the various parts of the study, was prepared with solutions that were not deaerated. Similarly, the mixing and stirring (30 seconds) of the solutions that led to the chukanovite precipitate was achieved without protection from air. Once obtained, the suspension was poured in a flask filled to the rim and the flask was hermetically sealed. The precipitate was finally aged for 1 week at room temperature (RT = 21±2 °C) before analysis or partial oxidation. This reference precipitate, aged 1 week, is called CF0 and was assumed to be close to Fe(II)-chukanovite (this point is thoroughly discussed in section 4.1).

Samples of chukanovite CF0 were also aged in suspension at RT for up to 8 months.

2.2. Oxidation of Fe(II)-chukanovite CF0 suspensions

A progressive partial oxidation of Fe(II)-chukanovite CF0 precipitates was achieved by a magnetic stirring (600 rpm, rod 4-cm long and 8-mm diameter) of the suspensions in the open air. The 300 mL suspensions were aerated at the liquid-air interface in a 600 mL beaker of 9-cm diameter. According to previous study [11], Fe(III)-containing chukanovite should be obtained as an intermediate transient compound before the end products of the oxidation process, i.e. Fe(III) oxyhydroxides, appear. The Fe(III) content able to accumulate in the

chukanovite structure during this process was estimated at 11-14% [11]. This estimation was obtained via the determination of the oxidation time t_F required for the formation of FeOOH phases (i.e. oxidation of 100% Fe^{II}) and the oxidation time t_I required for the formation of Fe(III)-containing chukanovite, assuming a constant oxidation rate.

Oxidation times of 15, 30 and 60 minutes were chosen according to previous work [11]. Before a time t_I ~ 55 minutes, the oxidation of Fe(II) did not lead to the formation of any additional solid phase and it was forwarded that the oxidation of Fe(II) took place in situ inside the crystal structure of chukanovite [11]. After time t_I, the formation of FeOOH phases began, possibly because the crystal structure of chukanovite could host no more Fe(III). At the end of the oxidation period, one half of the precipitate was filtered for analysis. The other half was left in suspension, sheltered from air as described in the previous section for Fe(II)-chukanovite CF0, to be analyzed after ageing. Each experiment was performed at least three times with ageing durations up to 10 months.

The pH of the suspension was measured in each case before and after the oxidation period using a glass electrode.

2.3. Co-precipitation of Fe(II) and Fe(III)

With the aim of preparing Fe(III)-containing chukanovite by co-precipitation of dissolved Fe(II) and Fe(III) species with carbonate and hydroxide ions, another procedure was used. It consisted in mixing a $FeSO_4 \cdot 7H_2O$ + $FeCl_3 \cdot 6H_2O$ solution with a NaOH + $Na_2CO_3 \cdot 10H_2O$ solution, with concentrations corresponding to the ratios [Fe(II)+Fe(III)]/[NaOH] = 1.0 and [$Na_2CO_3 \cdot 10H_2O$]/[NaOH] = 0.5 as for the formation of chukanovite (reaction 1). The considered amounts of Fe(III), expressed as $[Fe^{III}]/[Fe^{II} + Fe^{III}]$ concentration ratios (in %), were 2%, 5% and 10%. The maximal Fe(III) content of 10%

considered here is similar to that reported previously for Fe(III)-containing chukanovite [1,11].

All the samples were aged 1 week at RT using the procedure described in the previous section for Fe(II)-chukanovite CF0.

3. Methods

The precipitates were characterized by a combination of four techniques, namely X-ray diffraction (XRD), Transmission Mössbauer spectroscopy (TMS), Fourier-Transform Infrared (FTIR) spectroscopy and μ-Raman spectroscopy. The first aim was to identify all the phases, crystalline or not, possibly present with chukanovite in the precipitates. TMS was more specifically used to demonstrate that chukanovite could indeed contain some Fe(III) and to quantify this Fe(III) content. XRD data were thoroughly analyzed to confirm, via a possible evolution of lattice parameters, the presence of a variable amount of Fe(III).

3.1. XRD analysis

Since chukanovite is very sensitive to the oxidizing action of O_2, a specific procedure was used. The precipitate was filtered while being sheltered from air during the process with a plastic membrane. A slightly wet paste was then obtained.

XRD analysis was performed at RT with an Inel EQUINOX 6000 diffractometer, using a curved detector (CPS 590), with the Co-Kα radiation (λ = 0.17903 nm). The curved detector is designed for the simultaneous detection of the diffracted photons on a 2θ range of 90°. The calibration of the angular scale was made specifically for the present study using a standard sample of LaB_6. Acquisition was made with a constant angle of incidence (5 degrees) over 45 minutes. To prevent the oxidation of chukanovite during preparation and analysis, the slightly wet paste obtained after filtration was mixed with a few drops of

glycerol in a mortar. It was then crushed until a homogenous oily paste was obtained. With this procedure the various chukanovite particles are coated with glycerol and sheltered from the oxidizing action of O_2 [32,33].

To obtain a maximum of reliable information from the XRD data, Rietveld refinements [34] of the patterns were performed using the MAUD (Materials Analysis Using Diffraction) software [35]. With this software, the whole XRD patterns are fitted taking into account structural and microstructural parameters of the sample, and instrumental characteristics. Lattice parameters of chukanovite and phase composition of mixtures of magnetite and chukanovite were determined using this procedure. The reliability of the computer fitting is testified in each case by two factors, the weighted profile *R*-factor, R_{wp}, and the goodness of fit, χ^2 [36].

In any case, the signal due to glycerol was subtracted from the experimental data using an XRD pattern of glycerol acquired in the same experimental conditions. Such a data processing may have an influence, affecting in particular the intensity of the diffraction peaks. However, the only objective of the study was to observe the evolution of lattice parameters and phase composition with oxidation/ageing time. Consequently, only a comparison between the data obtained for various oxidation/ageing times was made and each XRD pattern was treated with the same procedure. To check the validity of this methodology, two XRD patterns of the same sample were treated so that the dispersion of computed parameters for a given sample could be determined. The results proved sufficiently accurate (see tables 2 and 4) to consider that the procedure used, if reproduced exactly the same way for each pattern, whether has no impact on the XRD data or has a systematic impact that influences similarly each XRD pattern.

3.2. Mössbauer spectroscopy analysis

TMS was performed at various temperatures, i.e. RT, 77 K and 8 K, with a constant acceleration Mössbauer spectrometer and 512 multichannel analyzer (Halder Electronic Gmbh), and a 50 mCi source of ^{57}Co in Rh maintained at RT and mounted at the end of a Mössbauer velocity transducer. Data were obtained from appropriate amounts (10 mg of Fe per cm^2) of solid samples to get optimal experimental conditions.

The samples were prepared under N_2 atmosphere in an anoxic glove box (Jacomex) and quickly transferred under inert He atmosphere to the cold head cryostat manufactured by Advanced Research Systems, equipped with vibration isolation stand, developed in LCPME laboratory (CNRS and Lorraine University, France). The calibration of the velocity scale was carried out for the study using the Mössbauer absorption lines of a reference absorber, i.e. α-iron, at RT. The Mössbauer spectrum of α-iron is a sextet with well known hyperfine parameters, which provides a calibration based on 6 points, i.e. the position of each peak of the sextet.

The TMS spectra were analyzed using the Recoil software [37]. Two approaches were used for this analysis. For the spectra obtained near and above 35 K the Lorentzian-shape lines model was adequate. The experimental spectra were then fitted with doublets corresponding to paramagnetic sites with a quadrupole splitting. For the spectra obtained at very low temperature, due to the appearance of a magnetic ordering for the Fe(II) components, the full static Hamiltonian site analysis was required for solving the mixed hyperfine interactions.

3.3. FTIR analysis

FTIR measurements were performed with a Thermo-Nicolet iS50 spectrometer using an iTX ATR (attenuated total reflectance) accessory with a diamond crystal. The apparatus is equipped with a KBr beamsplitter and a DTGS detector and monitored by the Omnic

software. It is checked each 6 months using the bench diagnosis function of the software, based on the ATSM E 1421-99 (Standard practice for describing and measuring performance of FTIR spectrometer level zero and level one tests). Furthermore, the wavenumber scale is checked each three months using a standard polystyrene film.

For the present study, the sample holder was covered by a cell insulating it and allowing a nitrogen flow to pass through. A background spectrum was acquired each hour and used for all sample spectra acquired within this hour. The validity of the background spectrum was however checked before each acquisition using the previsualization function of the Omnic software. This previsualization was performed before the sample was set on the diamond crystal of the ATR device, i.e. the signal had to be equal to zero if the background spectrum was still valid. The background spectra were acquired under nitrogen flow like those of the samples.

The slightly wet paste obtained after filtration (see section 3.1) was rinsed with water and ethanol while being sheltered from air. It was then rapidly set on the diamond crystal of the ATR accessory. After a complete evaporation of the ethanol remaining in the sample, verified via the previsualization function, the spectrum was recorded with a resolution of 8 cm^{-1} which proved sufficient to distinguish all the characteristic vibration bands of chukanovite [6]. 128 scans were acquired for each spectrum.

3.4. μ-Raman spectroscopy analysis

Raman analysis was performed on a Jobin Yvon High Resolution Raman spectrometer (LabRAM HR Evolution) equipped with a confocal microscope, a Peltier-based cooled charge coupled device (CCD) detector and a solid-state diode pumped green laser (532 nm). The apparatus is calibrated at least each 3 months using a Si wafer and more precisely the Raman peak of Si located at 520.5 cm^{-1}.

The slightly wet paste obtained after filtration (see section 3.1) was crushed between a glass plate and a very thin glass platelet so that the Fe(II)-compounds were sheltered from air during the acquisition of the spectrum. The laser was then focused on the sample through the thin glass platelet. Its power was reduced between 25% and 1% of the maximum (i.e. between 1.94 and 0.07 mW) because an excessive heating can induce the transformation of the analyzed Fe compounds into hematite α-Fe_2O_3. More precisely, the sample was first analyzed using the lower laser power, i.e. 1% of the maximum, to identify the main phases present in the sample. Then, to obtain high quality spectra that may reveal minor phases, several acquisitions were performed with increasing laser power, until a high signal to noise ratio was obtained. An excessive heating, i.e. an excessive laser power, is revealed by the presence of the well-known Raman peaks of hematite. In any case, the acquisition time did not exceed 2 minutes.

4. Experimental results

4.1. Characterization of Fe(II)-chukanovite CF0 after various times of ageing in suspension

Figure 1 shows the corresponding XRD pattern and FTIR spectrum of reference Fe(II)-chukanovite CF0 aged for 1 week. The XRD pattern (fig. 1a) is made of rather broad diffraction peaks, indicating a poor crystallinity. Moreover, these peaks are found on a broad hump, extending from $2\theta \sim 25°$ to $2\theta \sim 35°$, due to the presence of glycerol. Nevertheless, all visible diffraction peaks could be attributed to chukanovite (ICDD-JCPDS file 01-076-6357 corresponding to [2]), except for the one denoted by a star. Consequently, XRD analysis shows that chukanovite is the only detected crystalline phase. However, the presence of amorphous/nano-crystalline matter or minor phases cannot be discarded.

The full width at half maximum is the smallest for the 020 (and 12-1/021) peak, which indicates that chukanovite particles grew preferentially along the *b* axis of the monoclinic

crystal structure. This is consistent with the previous descriptions of chukanovite crystals, reported as acicular or fibrous [2] and acicular to platy [8].

Chukanovite is also the only solid phase detected by FTIR spectroscopy (fig. 1b). The signal observed between 1800 and 2300 cm^{-1} is due to the ATR device and does not correspond to a vibration band. The two broad peaks observed here are only artifacts located in the wavenumber regions where the diamond of the ATR device strongly absorbs the IR incident beam.All the other peaks are those reported previously for chukanovite [2,6,10,11] and interpreted as follows [6]: the bands at 3484 and 3322 cm^{-1} are attributed to OH stretching, those at 1540 and 1355 cm^{-1} to the ν_3 antisymmetric CO_3^{2-} stretching. The weaker band at 1100 cm^{-1} is attributed to ν_1 symmetric CO_3^{2-} stretching while those at 1054 and 955 cm^{-1} are due to δ OH deformation modes. The band at 837 cm^{-1} can be attributed whether to ν_2 CO_3^{2-} bending or δ OH deformation modes. Finally, the three last bands at 782, 695 and 654 cm^{-1} corresponds to ν_4 CO_3^{2-} bending modes. Because FTIR spectroscopy can detect crystalline phases and non-crystalline phases as well, this result shows that chukanovite is the only solid phase present in the precipitate.

The evolution over time of Fe(II)-chukanovite CF0 was also studied. Figure 2 shows the XRD pattern of a sample aged 8 months at RT. It is very similar to the previous one (fig. 1a) but some diffraction peaks of chukanovite are better defined (i.e. 001, 330, 250/511, 431 and 44-1) which indicates a slightly improved crystallinity. For instance, the FWHM of the peaks 210 and 020 decreased from 2.09° (201) and 0.85° (020) for unaged CF0 to 1.73° (210) and 0.45° (020) for aged CF0. The relative intensity of the non-interpreted diffraction line (*) is smaller, which indicates that its presence may be associated with the poor crystallinity, i.e. imperfect ordering, of the obtained chukanovite particles, or to the presence of a minor phase now disappeared. Fe(II)-chukanovite may be metastable with respect to siderite [9] but, in the

considered experimental conditions and after 8 months, it remained the only solid phase present.

Other analytical methods confirmed this result. As an example, TMS spectra of 2 months old chukanovite CF0, collected at 77 K and 8 K, are displayed in figure 3. At 77 K, the precipitate is in paramagnetic state and its spectrum only made of quadrupole doublets. The spectrum could be adequately fitted with two doublets characterized by the same center shift (CS) typical of ferrous state in high spin configuration, indicated by its value of 1.23 mm s^{-1} and two slightly different values for quadrupole splitting Δ, i.e. 2.09 and 2.56 mm s^{-1} (table 1). These two values are ascribable to the presence of two Fe(II) octahedral sites Fe1 and Fe2 [2,10]. The octahedral environment of Fe1 is made up of four oxygen atoms belonging to carbonate ions and two OH^- ions, whereas four OH^- ions and two oxygen atoms from CO_3^{2-} ions surround Fe2. The Fe1 octahedron is more distorted than the Fe2 octahedron [2]. In Mossbauer spectroscopy, the quadrupole splitting Δ arises from the second hyperfine interaction that is the interaction between quadrupole moment Q (due to non-spherical charge distribution of the nucleus) and electric field gradient (EFG). The EFG, caused by the spatial distribution of the electrons around the nucleus, has a strong relation to site symmetry and local structure. For chukanovite, the quadrupole doublet with the highest quadrupole splitting Δ must then correspond to the most distorted Fe1 octahedral site. The doublet with smaller quadrupole splitting Δ then corresponds to Fe2. The two doublets are found in similar proportion, in agreement with the crystal structure of chukanovite, where Fe(II) cations are present in equal proportions in the two octahedral sites [2,10].

The shape of the 8 K spectrum is more complex and completely different from that of the 77 K spectrum. It indicates that all the Fe(II) sites are magnetically ordered and are represented by octets (table 1). Modelling with the software package Recoil [37] of such a spectrum is complex because for Fe(II) compounds electric quadrupole and magnetic

hyperfine interactions are generally of the same order of magnitude and it is not to possible to analyze the spectrum with six line patterns (sextets) as it is usually done for Fe(III) compounds [38,39]. Each octet comprises eight lines that have to be fully computed by solving the eigenvalues of the Hamiltonian. Due to the considerable line broadening revealed by the experimental spectrum, we have improved the fitting of the low temperature spectrum by adding a paramagnetic component as a quadrupole doublet typical of Fe(III) but of very low intensity. However, this may be an artifact due to the complexity of the spectrum.

In conclusion, the precipitate CF0 proved to be composed of chukanovite as a major phase hosting a very low proportion of Fe(III) (if any), and did not transform over time in anoxic conditions, i.e. remained unchanged after 8 months of ageing in suspension at RT except for a slight increase of crystallinity. In the following, CF0 is then considered as the reference Fe(II)-chukanovite.

4.2. Synthesis and characterization of Fe(III)-containing chukanovite

Precipitates CF0 were aged for 1 week and subsequently exposed to air in a beaker, as described in section 2.3, for 15, 30 or 60 minutes. The pH of the initial CF0 suspensions was measured at 9.6±0.2. The oxidation process was accompanied by a decrease of pH, as already observed [11]. After the 15-minute oxidation period, the pH was measured at 9.5 ± 0.2, i.e. was similar to the initial pH. After the 30-minute oxidation period, an important discrepancy was observed from one experiment to another, leading to an average value of 9.0±0.4. After the 60-minute oxidation period, the pH was significantly lower, at 7.8±0.2. According to previous study [11], this rapid decrease of pH, occurring between 30 and 60 minutes of oxidation, is associated with the beginning of the formation of FeOOH phases.

Figure 4 displays the corresponding XRD patterns. After 15 minutes of exposure to air, only the diffraction lines of chukanovite are seen, in agreement with previous work [11].

Because an exposure to air of 15 minutes necessarily implies that part of the Fe(II) cations are oxidized to Fe(III), the absence of any other compound suggests that the oxidation process only involved an in-situ oxidation of Fe(II) cations inside the chukanovite structure. Note that the oxidation process leads to visible effects: the color of the suspension turned to a slightly darker shade of grey after the 15 minutes exposure to air.

After 30 minutes of exposure to air, the main diffraction lines of goethite (α-FeOOH), one of the end products of the oxidation of chukanovite [11,12], were observed in some samples (G_{111} and G_{110}, corresponding respectively to I_{110} = 100, d_{110} = 4.14 Å and I_{111} = 50, d_{111} = 2.45 Å according to ICDD-JCDS file No 00-29-0713). In other samples, they were not observed (data not shown) and it is then questionable whether the small amount of goethite, when detected, resulted from the 30-minute oxidation of the aqueous suspension or has formed during the preparation (filtration...) and analysis of the sample.

After 60 minutes of exposure to air, the two main diffraction lines of goethite were clearly seen in any case. This means that at 60 minutes of exposure to air the second oxidation stage of chukanovite, i.e. the formation of FeOOH phases, has already begun.

Figure 4 clearly shows a shift of the main diffraction line of chukanovite with increasing oxidation time. This suggests that the increasing Fe(III) content induces changes of the lattice parameters of the chukanovite structure. Table 2 gathers the lattice parameters determined for chukanovite after 1 week of ageing with and without subsequent oxidation. As explained in section 3.1, only the influence of the oxidation time is to be discussed. It can then be observed that the lattice parameter *c* appears rather constant, only varying between 3.190 Å for 15 minutes of oxidation and 3.205 Å for 60 minutes of oxidation. However, clear trends are observed for the other lattice parameters. In particular, lattice parameter *b* decreases significantly, from 9.37 Å to 9.16 Å, with increasing oxidation time. The angle β decreases from 97.04° to 95.1° while the lattice parameter *a* increases with increasing oxidation time.

These variations of the lattice parameters, linked to the oxidation time, can be attributed to the increasing Fe(III) content of chukanovite. Actually, the ionic radius of Fe^{3+} is smaller than that of Fe^{2+}, with 0.645 Å instead of 0.78 Å [40]. The decrease of the lattice parameter *b* may then be due to the decrease of the average ionic radius of the Fe cations as the proportion of Fe(III) increases. The increase of the lattice parameter *a* , associated with the decrease of the angle β, however reveals a strongly anisotropic behavior of the cell parameters as a result of the substitution of Fe(II) to Fe(III) and the corresponding substitution of 1 OH^- to 1 O^{2-} ion in the surrounding octahedron of oxygen atoms. This anisotropic behavior of cell parameters must be linked to structural features of chukanovite. A similar example was reported for cobaltoan malachites [41].

The oxidized precipitates were also analyzed by other methods. Figure 5 displays as an example the FTIR spectrum of a precipitate oxidized 30 minutes by air. This spectrum is typical of chukanovite. Goethite, as well as any other FeOOH compound, was not detected. FTIR analysis confirms that the 30 minutes of oxidation have mainly led to an in situ oxidation of Fe(II) cations inside the crystal structure of chukanovite. This duration can then be considered as the maximum oxidation time that, in our experimental conditions, can lead to a single phase system, i.e. a precipitate only composed of Fe(III)-containing chukanovite. For 60 minutes of oxidation, a two-phase system, i.e. Fe(III)-containing chukanovite + goethite, was obtained in any case.

Mossbauer analysis was then focused on samples oxidized 30 minutes. The analysis was performed at RT and 77 K and the obtained spectra are displayed in figure 6. Both spectra are mainly composed of two Fe(II) quadrupole doublets characterized by large CS and quadrupole splitting values (table 3) and one Fe(III) doublet, characterized by smaller CS and Δ values. The parameters obtained at 77 K for the Fe(II) doublets are similar to those obtained for sample CF0 at the same temperature (see table 2) and can then be assigned to chukanovite.

They are found at both temperatures in a ratio Fe1:Fe2 = 1 in agreement with the crystal structure of chukanovite (see also section 4.1). The Fe(III) doublet, present at both temperatures, cannot be attributed to goethite. Actually, goethite is magnetically ordered at RT and should give rise to a sextet characterized by a small CS of 0.53 mm/s, a quadrupole splitting Δ close to zero and a hyperfine field of 360 kOe [42,43]. However, microcrystalline goethite is often characterized by a superparamagnetic behavior at RT, i.e. may give rise to a paramagnetic doublet, due to small particle size [44]. It however tends to order magnetically when the temperature is lowered and give rise to a magnetically split sextet at 77 K [43,45]. This sextet is not observed here, i.e. TMS shows that goethite was not present in this sample.

The observed Fe(III) doublet can then be attributed to the Fe(III) cations present in the crystal structure of chukanovite. Its quadrupole splitting is high (for Fe^{III} state), indicating a strongly distorted environment. The obtained values of 0.87 mm/s (RT) and 0.74 mm/s (77 K) are for instance significantly higher than those of Fe(III) in GR compounds, e.g. 0.45 mm/s at 77 for GR(SO_4^{2-}) [46] or in lepidocrocite γ-FeOOH, i.e. 0.55 mm/s at 77 K [47]. High quadrupole splitting values are found for ferrihydrite (0.7 – 0.85 mm/s [48]), a poorly crystalized and poorly ordered Fe(III) oxyhydroxide where the sites are also highly distorted. It must also be noted that the Fe1:Fe2 ratio remains equal to 1 in Fe(III)-containing chukanovite, which implies that the Fe(III) cations are equally distributed in both octahedral sites. The unique Fe(III) doublet used for the interpretation of the spectra then corresponds to both Fe(III)1 and Fe(III)2 sites.

The proportion of Fe(III) present in the crystal structure of chukanovite after 30 min. of oxidation is then estimated at 11-13% by TMS (table 3). A similar Fe(III) content was previously reported [1,11].

4.3. Evolution of Fe(III)-containing chukanovite suspensions under anoxic conditions

The precipitates obtained after 15, 30 and 60 minutes of oxidation by air were aged 10 months in anoxic conditions. The results of the XRD analysis of the precipitates after ageing are summarized in figures 7-9. The precipitate oxidized 15 minutes by air was initially only composed of Fe(III)-containing chukanovite (fig. 4). After ageing (fig. 7a), the diffraction lines of magnetite Fe_3O_4 are clearly seen. In section 4.1, it was observed that the ageing of Fe(II)-chukanovite CF0 precipitates only induced a slight increase of crystallinity. The formation of magnetite during the ageing of the precipitate must then be attributed to the transformation of Fe(III)-containing chukanovite. Because only magnetite and chukanovite are present, this transformation more likely leads to magnetite and Fe(II)-chukanovite, i.e. the Fe(III) cations are expelled from the chukanovite structure to form magnetite. The reaction can be written as follows:

$$4Fe^{II}_{2-x}Fe^{III}_{x}(OH)_{2-x}O_xCO_3 + 2xH_2O \rightarrow$$

$$(4-3x)Fe^{II}_2(OH)_2CO_3 + 2xFe^{II}Fe^{III}_2O_4 + 6xH^+ + 3xCO_3^{2-} \quad (5)$$

Because the crystal structure of magnetite differs strongly from that of chukanovite, reaction (5) is not likely to take place through a solid-state transformation and a dissolution-reprecipitation process can be reasonably proposed.

The ageing of the precipitate oxidized 30 minutes also led to the formation of magnetite. A detailed view of the 32°-46° angular region of its XRD pattern is compared in fig. 7b with that of the precipitate oxidized 15 minutes. It can clearly be seen that the intensity of the M220 and M311 diffraction lines of magnetite increase with the oxidation time. This confirms that the amount of magnetite due to ageing is associated with the Fe(III) amount initially present in chukanovite, i.e. that magnetite comes from the transformation of Fe(III)-containing chukanovite.

The Rietveld refinements of the XRD patterns confirmed this analysis. The results are listed in table 4 and two computed patterns (oxidation times of 15 min. and 60 min.) are

compared to experimental data in figure 8 to illustrate the accuracy of the fitting. The proportion of magnetite is found to increase with the oxidation time, from 2 % for 15 min. oxidation to 5 % for 30 min oxidation and finally 12 % for 60 min. oxidation. The amount of goethite present after 60 min. oxidation is about 9%. If we assume that magnetite comes from the transformation of Fe(III)-containing chukanovite, then the Fe(III)-containing chukanovite present in the sample oxidized 60 minutes would have contained more Fe(III) than the Fe(III)-containing chukanovite present in the sample oxidized 30 minutes. This is consistent with the evolution of the lattice parameters with the oxidation time (see table 2) that still vary from 30 to 60 minutes of oxidation.

The lattice parameters *a* and *b* of chukanovite after the 10 month ageing period (table 4) still depend on the oxidation time but their variations are less significant. This confirms that the formation of magnetite, i.e. reaction (5), has indeed led to a significant decrease of the Fe(III) content of chukanovite. Parameter *b*, which varied from 9.31 Å (15 min. oxidation) to 9.16 Å (60 min. oxidation) before ageing, varies from 9.34 Å (15 min. oxidation) to 9.30 Å (60 min. oxidation) after ageing. In each case, parameter *b* has increased and parameter *a* has decreased after ageing. The β angle is even constant at 98(± 0.1)°. It was observed (table 2), that the increase of the oxidation time, i.e. the Fe(III) content, led to a decrease of *b*, an increase of *a* and a decrease of β. The evolution of the lattice parameters during ageing is indeed consistent with a decrease of the Fe(III) content.

The transformation of Fe(III) chukanovite was also followed over time. In figure 9, the XRD patterns of precipitates oxidized for 15 minutes by air and subsequently aged 15 minutes, 7 days and 10 months are compared. The 7 main diffraction lines of magnetite are seen for the sample aged 10 months. None of the magnetite diffraction lines is seen after 15 minutes of ageing while only the main one, M311, is detected after 7 days of ageing. This shows that the transformation of Fe(III)-chukanovite is only partial, in our experimental

conditions, after 1 week. The transformation rate of Fe(III)-containing chukanovite is sufficiently low so that this compound can persist at that time scale.

Other analytical tools led to consistent results. As an example, two Raman spectra are shown in figure 10. They are both representative of the numerous spectra acquired during the analysis of these samples. Raman analysis is performed locally on a 5-6 µm diameter region of the considered precipitate. It is a local analysis but it appeared that the precipitates, composed of much smaller particles, were rather homogeneous at that scale. In the case of a multiphase system, each Raman spectrum proved composed of the spectral components of each phase, with only the respective intensity of the vibration bands associated with the different phases varying from one spot to another. The first spectrum (fig. 10a) is that of reference Fe(II)-chukanovite CF0 after two weeks of ageing. The only solid phase identified is indeed chukanovite, characterized here by its main Raman band at 1071 cm^{-1} [3-6]. The other sharp peak at 981 cm^{-1} is attributed to sulfate ions. These ions are whether present in solution (wet precipitates were analyzed) or adsorbed on chukanovite particles. The broad humps at ~450 cm^{-1} and ~950 cm^{-1} are due to the thin glass platelet that shelters the precipitate from air.

The second spectrum (fig. 10b) is that of the precipitate oxidized 60 minutes by air and subsequently aged 1 month in anoxic conditions. Magnetite is identified by its main Raman band at 673 cm^{-1} [49,50], indicating that the transformation of Fe(III)-containing chukanovite has already led to detectable effects. Goethite is identified by two intense bands at 302 cm^{-1} and 387 cm^{-1} and three smaller ones at 243 cm^{-1} and 485 cm^{-1} [49,50]. This phase was already present after the 60-minute oxidation period (fig. 4).

4.4. Characterization of the precipitates obtained from Fe(II) and Fe(III) salts

The results can be summarized by the description of the XRD analysis. Because of the poor crystallinity of chukanovite, a well crystallized phase present with chukanovite is easily detected on the XRD patterns, as illustrated by figure 11. The whole XRD pattern of the precipitate obtained with 5% Fe(III) is presented in figure 11a. The characteristic (broad) diffraction peaks of chukanovite are accompanied by thin and sharp lines of the sulfated green rust $GR(SO_4^{2-})$ [51], i.e. the Fe(II-III) double layered hydroxysulfate with chemical formula $Fe^{II}_4 Fe^{III}_2 (OH)_{12} SO_4 \cdot 8H_2O$ [51].

In figure 11b, a detailed view of the 5°-35° angular region, where the 3 main diffraction peaks of $GR(SO_4^{2-})$ are located, is presented for the precipitates obtained with 2%, 5% and 10% of Fe(III). In any case, the GR_{hkl} lines are clearly observed, even with only 2% of Fe(III). The intensity of those lines increases with the proportion of Fe(III). More precisely, the intensity of the GR_{001} peak, determined via a fitting of the experimental curves with a Gauss function, was found to increase from 800 to 2200 and 4100 (arbitrary unit) with Fe(III) content increasing from 2% to 5% and 10%. This shows that the amount of $GR(SO_4^{2-})$ is roughly proportional to the quantity of Fe(III) available in the system (i.e. 800×2.5 = 2000 and 800×5 = 4000).

In conclusion, the presence of Fe(III) in solution has mainly induced, in the considered experimental conditions, the formation of $GR(SO_4^{2-})$. The Fe(II-III) hydroxysulfate was obtained as a consequence of the high sulfate concentration of the medium. Chloride ions were also present but $GR(Cl^-)$ did not form, in agreement with previous work [33], because the layered structure of GRs has a greater affinity for sulfate ions, and more generally for divalent anions that give the structure a greater stability [52,53]. In the presence of Fe(III) and sulfate species, the precipitation reaction leading to a mixture of chukanovite and $GR(SO_4^{2-})$ can be written as follows:

$$(12\text{-}6x)Fe^{2+} + 6xFe^{3+} + 12OH^- + 6CO_3^{2-} + 3xSO_4^{2-} + 24xH_2O \rightarrow$$

$$(6\text{-}18x)Fe^{II}_2(OH)_2CO_3 + 3xFe^{II}_4\,Fe^{III}_2\,(OH)_{12}\,SO_4\cdot 8H_2O + 18xFe^{2+} + 18xCO_3^{2-} \quad (4)$$

As such, the proportion of Fe(III), that is $[Fe^{3+}]/([Fe^{2+}]+[Fe^{3+}])$, is equal to $6x/(12-6x+6x)$, that is $x/2$. The Fe(III) proportions considered here, i.e. 2%, 5% and 10%, then correspond to x = 0.04, 0.1 and 0.2. The amount of $GR(SO_4^{2-})$ formed is $3x$, i.e. is proportional to the amount of Fe(III).

According to reaction (4), OH^- ions are lacking so that part of the Fe^{2+} cations should be left in solution with a corresponding amount of carbonate ions. These species could lead to siderite $FeCO_3$ that was however not detected. Similar results, i.e. absence of siderite while Fe^{2+} and CO_3^{2-} ions are left in excess in solution together with chukanovite, were already reported [6,9]. The CO_3^{2-} ions left in excess in solution can react with water molecules to produce HCO_3^- and OH^- ions, thus leading to alkaline conditions that were assumed to inhibit the formation of siderite [6,9].

One can finally notice that even for 10% Fe(III), chukanovite is still the major phase; it would represent (using x = 0.2 in equation 4) 4.8 moles of Fe for 3.6 moles of Fe in $GR(SO_4^{2-})$.

5. Discussion

Fe(III)-containing chukanovite could only be obtained by oxidation of Fe(II)-chukanovite precipitates. It was mixed with α-FeOOH for an oxidation time of 60 minutes but was the only solid phase for oxidation times up to 30 minutes, with a maximum Fe(III) content of 11-13%. When Fe(II) and Fe(III) salts were used, the obtained precipitate consisted of a mixture of Fe(II)-chukanovite and $GR(SO_4^{2-})$. In this case, the Fe(III) cations marginally participated to the building up of the chukanovite structure. These results show that Fe^{3+} cations can be present in this structure only if they result from the in-situ oxidation of Fe^{2+} cations already present in the crystal structure.

Fe(III)-containing chukanovite transformed in anoxic conditions into a mixture of Fe(II)-chukanovite and magnetite, which shows that the two-phase system $Fe^{II}_2(OH)_2CO_3$ + $Fe^{II}Fe^{III}_2O_4$ is more stable than the one-phase system $Fe^{II}_{2-x}Fe^{III}_x(OH)_{2-x}O_xCO_3$ in the considered experimental conditions. In section 4.4, it was observed that the co-precipitation of Fe(II) and Fe(III) also led to a two-phase system, in this case $Fe^{II}_2(OH)_2CO_3$ + GR(SO_4^{2-}). According to available thermodynamic data and previous experimental results [54], GR(SO_4^{2-}) is metastable with respect to magnetite. The most stable system is then more likely the two-phase system $Fe^{II}_2(OH)_2CO_3$ + $Fe^{II}Fe^{III}_2O_4$, the other two-phase system $Fe^{II}_2(OH)_2CO_3$ + GR(SO_4^{2-}) being obtained as a result of the co-precipitation process due to the fast kinetic it implies.

In contrast, Fe(II)-chukanovite did not transform after 8 months in anoxic conditions, though it is metastable with respect to siderite [9]. This is consistent with its common identification as a corrosion product on ferrous archaeological artifacts [3-6]. In such ancient systems, chukanovite is in most cases associated with siderite. This suggests that the transformation of Fe(II)-chukanovite to siderite could be very slow and lead to significant effects only at very long term, i.e. not after a few months. Magnetite was not observed either. This result suggests that in anoxic conditions, Fe(II)-chukanovite cannot be oxidized into Fe(III)-containing chukanovite. The presence of Fe^{3+} cations inside the crystal structure of chukanovite requires an oxidizer stronger than H_2O, e.g. dissolved O_2 as illustrated by our results. In actual corrosion systems (nuclear waste, storage, buried archaeological artefacts, permeable reactive barriers…) the formation of Fe(III)-containing chukanovite could then only result from isolated and/or moderate O_2 ingress.

Therefore, according to these results, Fe(III)-containing chukanovite may only persist for days or maybe weeks. Consequently, whatever its possible electrical conductivity, it does not seem able to play an important role in long-term corrosion processes such as those studied

in the frame of nuclear waste management in deep geological disposals. Actually, a recent study of the electrical properties of rust layers containing chukanovite revealed that this compound behave as an insulator [55].

Fe(III)-containing chukanovite may however be involved as a transient phase in redox processes occurring at a smaller time scale (e.g. a few days). It is also possible that in some cases, the transformation of Fe(III)-containing chukanovite could be inhibited, e.g. via the adsorption of strongly bound molecules/ions on Fe(III)-containing chukanovite particles, which may prevent the dissolution-reprecipitation process leading to the two phase system $Fe^{II}_2(OH)_2CO_3 + Fe^{II}Fe^{III}_2O_4$.

The transformation of Fe(III)-chukanovite in anoxic conditions however leads to magnetite that is a well-known electronic conductor. More precisely, it may lead to the formation of numerous small magnetite particles scattered in a matrix of Fe(II)-chukanovite. Such magnetite "islets", already observed inside the corrosion product layer covering archaeological artefacts [55-57], may favor the decoupling of anodic and cathodic reactions and contribute actively to the corrosion process. This decoupling was observed in some cases and the presence of a network of nanometric magnetite particles connecting the metal to the outer part of the corrosion product layer was forwarded [57].

6. Conclusions

- Fe(III)-containing chukanovite could not be prepared by precipitation from Fe(II) and Fe(III) dissolved species. The Fe(III) species were mainly incorporated into a green rust compound, i.e. $GR(SO_4^{2-})$ in the considered experimental conditions, and Fe(II)-chukanovite precipitated from the excess Fe(II) species.

- Fe(III)-containing chukanovite could only be obtained via the oxidation (by dissolved O_2) of Fe(II) cations already present in the crystal structure. The amount of Fe(III)

present in chukanovite after 30 minutes of oxidation could be estimated by TMS analysis at 11-13%. Subsequent oxidation led to the formation of an additional Fe(III)-bearing phase, i.e. goethite.

- The increasing oxidation time of chukanovite led to significant variations of the lattice parameters, in particular to a contraction in the *b* direction, due to the increasing Fe(III) content.

- Fe(III)-containing chukanovite proved metastable in the considered experimental anoxic conditions. It tends to transform during ageing into a mixture of magnetite and Fe(II)-chukanovite. This shows that Fe(III)-containing chukanovite, whatever its electrical conductivity, is not likely to play an important role in corrosion systems at long term. It may however have an indirect influence though its transformation, that can favor the formation of magnetite particles scattered in the corrosion product layer.

Acknowledgements: This work is part of the PhD thesis of Julien DUBOSCQ financially supported by the "Communauté d'Agglomération de La Rochelle" (CDA La Rochelle) and part of the CPER/FEDER project "DYPOMAR".

References

[1] E. Erdös E., H. Altorfer, Ein dem Malachit ähnliches basisches Eisenkarbonat als Korrosionsprodukt von Stahl, Werkstoffe und Korrosion 27 (1976) 304-312.

[2] I.V. Pekov, N. Perchiazzi, S. Merlino, V.N. Kalachev, M. Merlini, A.E. Zadov, Chukanovite, $Fe_2(CO_3)(OH)_2$, A new mineral from the weathered iron meteorite Dronino, Eur. J. Mineral. 19 (2007) 891-898.

[3] M. Saheb, D. Neff, P. Dillmann, H. Matthiesen, E. Foy, Long-term corrosion behaviour of low-carbon steel in anoxic environment: Characterisation of archaeological artefacts, J. Nuclear Mat. 379 (2008) 118-123.

[4] M. Saheb, D. Neff, P. Dillmann, H. Matthiesen, E. Foy, L. Bellot-Gurlet, Multisecular corrosion behaviour of low carbon steel in anoxic soils: Characterisation of corrosion system on archaeological artefacts, Materials and Corrosion 60 (2009) 99-105.

[5] M. Saheb, D. Neff, L. Bellot-Gurlet, P. Dillmann, Raman study of deuterated iron hydroxycarbonate to assess long-term corrosion mechanisms in anoxic soils, J. Raman Spectroscopy 42 (2011) 1100-1108.

[6] C. Rémazeilles, Ph. Refait, Fe(II) hydroxycarbonate $Fe_2(OH)_2CO_3$ (Chukanovite) as iron corrosion product: Synthesis and study by Fourier Transform Infrared Spectroscopy, Polyhedron 28 (2009) 749–756.

[7] T. Nishimura, J. Dong, Corrosion behavior of carbon steel for overpack in groundwater containing bicarbonate ions, J. Power and Energy Systems 3 (2009) 23-30.

[8] T. R. Lee, R. T. Wilkin, Iron hydroxy carbonate formation in zerovalent iron permeable reactive barriers: Characterization and evaluation of phase stability, Journal of Contaminant Hydrology 116 (2010) 47–57.

[9] I. Azoulay, C. Rémazeilles, Ph. Refait, Determination of standard Gibbs free energy of formation of chukanovite and Pourbaix diagrams of iron in carbonated media, Corros. Sci. 58 (2012) 229-236.

[10] I. Pignatelli, E. Mugnaioli, R. Mosser-Ruck, O. Barres, U. Kolb, N. Michau, A multi-technique, micrometer- to atomic-scale description of a synthetic analogue of chukanovite, $Fe_2(CO_3)(OH)_2$, Eur. J. Mineral. 26 (2014) 221-229.

[11] I. Azoulay, C. Rémazeilles, Ph. Refait, Corrosion of steel in carbonated media: the oxidation processes of chukanovite ($Fe_2(OH)_2CO_3$), Corros. Sci. 85 (2014) 101-108.

[12] I. Azoulay, C. Rémazeilles, Ph. Refait, Oxidation of chukanovite ($Fe_2(OH)_2CO_3$): Influence of the concentration ratios of reactants, Corros. Sci. 98 (2015) 634-642.

[13] M. Schlegel, C. Bataillon, C. Blanc, D. Pret, E. Foy, Anodic Activation of Iron Corrosion in Clay Media under Water-Saturated Conditions at 90 °C: Characterization of the Corrosion Interface, Environ. Sci. Technol. 44 (2010) 1503–1508.

[14] A. Romaine, R. Sabot, M. Jeannin, S. Necib, Ph. Refait, Electrochemical synthesis and characterization of corrosion products on carbon steel under argillite layers in carbonated media at 80◦C, Electrochim. Acta 114 (2013) 152-158.

[15] M.L. Schlegel, C. Bataillon, F. Brucker, C. Blanc, D. Prêt, E. Foy, M. Chorro, Corrosion of metal iron in contact with anoxic clay at 90°C: Characterization of the corrosion products after two years of interaction, Appl. Geochem. 51 (2014) 1-14.

[16] A. Romaine, M. Jeannin, R. Sabot, S. Necib, Ph. Refait, Corrosion processes of carbon steel in argillite: Galvanic effects associated with the heterogeneity of the corrosion product layer, Electrochim. Acta 182 (2015) 1019-1028.

[17] Y. Leon, M. Saheb, E. Drouet, D. Neff, E. Foy, E. Leroy, J.J. Dynes, P. Dillmann, Interfacial layer on archaeological mild steel corroded in carbonated anoxic environments studied with coupled micro and nano probes, Corros. Sci. 88 (2014) 23-35.

[18] R.T. Wilkin, R.W. Puls, Capstone Report on the Application, Monitoring and Performance of Permeable Reactive Barriers for Ground Water Remediation. Performance Evaluations at Two Sites. EPA/600/R-03/045a. Office of Research and Development, Cincinnati, OH. 140 pp (2003).

[19] T. Kohn, K. Livi, A.L. Roberts, P. Vikesland, Longevity of granular iron in groundwater treatment processes: Corrosion product development, Environ. Sci. Technol. 39 (2005) 2867-2879.

[20] S.-W Jeen, J.L. Jambor, D.W. Blowes, R.W., Gillham, Precipitates on granular iron in solutions containing calcium carbonate with trichloroethene and hexavalent chromium. Environ. Sci. Technol. 41 (2007) 1989–1994.

[21] R.K. Kukkadapu, J.M. Zachara, J.K. Fredrickson, D.W. Kennedy, A.C. Dohnalkova, D.E. Mccready, Ferrous hydroxy carbonate is a stable transformation product of biogenetic magnetite, Amer. Min. 90 (2005) 151-515.

[22] Ph. Refait, M. Abdelmoula, F. Trolard, J.M. Génin, J.J. Ehrhardt, G. Bourrié, Mössbauer and XAS study of a green rust mineral ; the partial substitution of Fe^{2+} by Mg^{2+}, Amer. Min. 86 (2001) 731-739.

[23] Ph. Refait, M. Reffass, J. Landoulsi, R. Sabot, M. Jeannin, Role of nitrite species during the formation and transformation of the Fe(II-III) hydroxycarbonate Green Rust, Colloids Surf. A: Physicochem. Eng. Aspects 459 (2014) 225-232.

[24] K. Dideriksen, C. Frandsen, N. Bovet, A.F. Wallace, O. Sel, T. Arbour, A. Navrotsky, J.J. De Yoreo, J.F. Banfield, Formation and transformation of a short range ordered iron carbonate precursor, Geochim. Cosmochim. Acta 164 (2015) 94-109.

[25] J. Han, S. Nešić, B.N. Brown, Galvanic model for localized CO_2 corrosion, NACE Corrosion/08 Conference, paper n°2687 (2008).

[26] J. Han, D. Young, S. Nešić, Characterization of the passive film on mild steel in CO_2 environments, NACE Corrosion/08 Conference, paper n°2511 (2008).

[27] S.M. Wilhem, Galvanic corrosion caused by corrosion products, in Galvanic Corrosion, ASTM STP 978, Harvey P. Hack, Ed. American Society for Testing and Materials, Philadelphia, (1988) 23-34.

[28] A.M. Al-Mayouf, N.A. Al-Mobarak, A.A. Al-Swayih, Dissolution of magnetite coupled with iron of various surface areas, Corrosion 63 (2007) 916.

[29] A.M. Al-Mayouf, Dissolution of magnetite coupled galvanically with iron in environmentally friendly chelant solutions, Corrosion Science 48 (2006) 898-912.

[30] M. Robineau, A. Romaine, R. Sabot, M. Jeannin, V. Deydier, S. Necib, Ph. Refait, Galvanic corrosion of carbon steel in anoxic conditions at 80°C associated with a heterogeneous magnetite (Fe_3O_4) / mackinawite (FeS) layer, Electrochim. Acta 255 (2017) 274-285.

[31] C. Ruby, C. Upadhyay, A. Géhin, G. Ona-Nguema, J.-M.R. Génin, In situ redox flexibility of Fe^{II-III} oxyhydroxycarbonate green rust and fougerite, Environ. Sci. Technol. 40 (2006) 4696-4702.

[32] H.C.B. Hansen, Composition, stabilisation, and light absorption of Fe(II)-Fe(III) hydroxycarbonate (green rust), Clay Miner. 24 (1989) 663-669.

[33] Ph. Refait, R. Sabot, M. Jeannin, Role of Al(III) and Cr(III) on the formation and oxidation of the Fe(II-III) hydroxysulfate Green Rust, Colloids Surf. A: Physicochem. Eng. Aspects 531 (2017) 203-212.

[34] H. M. Rietveld, A profile refinement method for nuclear and magnetic structures, J. Appl. Crystallogr. 2 (1969) 65-71.

[35] L. Lutterotti, Maud: a Rietveld analysis program designed for the internet and experiment integration, Acta Cryst. A56 (2000) s54.

[36] R.A. Young, "Introduction to the Rietveld method," *The Rietveld Method*, edited by R.A. Young, Oxford University Press, Oxford, 1993, pp. 1–38.

[37] K. Lagarec, D. G. Rancourt, *Mössbauer analysis software Recoil*; University of Ottawa.

[38] B. Rusch, J.M. R. Génin, C. Ruby, M. Abdelmoula, P. Bonville, Ferrimagnetic properties in Fe $^{II-III}$ (oxy)hydroxycarbonate green rusts, Solid State Sci. 10 (2008) 40-49.

[39] B. Maitte, F.P.A. Jorand, D. Gregic, M. Abdelmoula, C. Carteret, Remineralization of ferrous carbonate from bioreduction of natural goethite in the Lorraine iron ore (Minette) by *Shewanella putrefaciens*, Chem. Geol. 412 (2015) 48-58.

[40] R. D. Shannon, Revised effective ionic radii and systematic studies of interatomic distances in halides and chalcogenides, Acta cryst. A32 (1976) 751-767.

[41] N. Perchiazzi, R. Dragone, N. Demitri, P. Vignola, C. Biagioni, Incorporation of Co in the rosasite–malachite carbonate group of minerals: crystal structure studies of kolwezite and synthetic cobaltoan malachites, Eur. J. Mineral. 30 (2018) 609–620.

[42] M.J. Rossiter, A.E.M. Hodgson, A Mössbauer study of ferric oxy-hydroxide, J. Inorg. Nucl. Chem. 27 (1965) 63-71.

[43] E. Murad, The characterization of goethite by Mössbauer spectroscopy, Amer. Min. 67 (1982) 1007-1011.

[44] M.B. Madsen, S. Morup, Asymmetric doublet in Mössbauer spectra of superparamagnetic goethite, Hyperfine Interactions 42 (1988) 1059-1062.

[45] C.J.W. Koch, M.B. Madsen, S. Morup, Decoupling of magnetically interacting crystallites of goethite, Hyperfine Interactions 28 (1986) 549-552.

[46] J.-M.R. Génin, A.A. Olowe, Ph. Refait, L. Simon, On the stoichiometry and Pourbaix diagram of Fe(II)-Fe(III) hydroxy-sulphate or sulphate-containing green rust 2; an electrochemical and Mössbauer spectroscopy study, Corros. Sci. 38 (1996) 1751-1762.

[47] C.E. Johnson, Antiferromagnetism of γ-FeOOH: a Mössbauer effect study, J. Phys. C 2 (1969) 1996-2002.

[48] E. Murad, The Mössbauer spectrum of well-crystallized ferrihydrite, J. Magn. Magn. Mater. 74 (1988) 153-157.

[49] D.L.A. De Faria, S.V. Silva, M.T.D. Oliveira, Raman micro spectroscopy study of some iron oxides and oxyhydroxides, J. Raman Spectroscopy 28 (1997) 873-878.

[50] D. Neff, P. Dillmann, L. Bellot-Gurlet, G. Beranger, Corrosion of iron archaeological artefacts in soil: characterisation of the corrosion system, Corros. Sci. 47 (2005) 515-535.

[51] L. Simon, M. François, Ph. Refait, G. Renaudin, M. Lelaurain, J.M. Génin, Structure of the Fe(II-III) layered double hydroxysulphate green rust two from Rietveld analysis, Solid State Sci. 5 (2003) 327-334.

[52] S. Miyata, Anion-exchange properties of hydrotalcite-like compounds, Clays Clay Miner. 31 (1983) 305-311.

[53] Ph. Refait, S.H. Drissi, J. Pytkiewicz, J.-M. Génin, The anionic species competition in iron aqueous corrosion: role of various green rust compounds, Corros. Sci. 39 (1997) 1699-1710.

[54] Ph. Refait, A. Géhin, M. Abdelmoula, J.M. Génin, Coprecipitation thermodynamics of iron(II-III) hydroxysulphate green rust from Fe(II) and Fe(III) salts, Corros. Sci. 45 (2003) 656-676.

[55] F. Mercier-Bion, Jiaying Lia, H. Lotz, L. Tortech, D. Neff , Ph Dillmann, Electrical properties of iron corrosion layers formed in anoxic environments at the nanometer scale, Corros. Sci. 137 (2018) 90-110.

[56] M. Saheb, D. Neff, E. Foy, J. Demory, P. Dillmann, Characterisation of the corrosion layers formed on ferrous archaeological artefacts buried in anoxic media, Corros. Eng. Sci. Technol. 45 (2010) 381–387.

[57] M. Saheb, D. Neff, C. Bataillon, E. Foy, Ph. Dillmann, Copper tracing to determine the micrometric electronic properties of a thick ferrous corrosion layer formed in an anoxic medium, Corros. Sci. 53 (2011) 2201-2207.

Figure captions

Figure 1: Analysis of reference Fe(II)-chukanovite CF0 after one week of ageing at RT: XRD pattern (a) and FTIR spectrum (b). The main diffraction peaks of chukanovite are indexed with the corresponding Miller index. On the IRTF spectrum, the vibration bands of chukanovite are denoted by their position in cm^{-1}.

Figure 2: XRD pattern of reference Fe(II)-chukanovite CF0 after 8 months of ageing at RT. The main diffraction peaks of chukanovite are denoted by the corresponding Miller index.

Figure 3: TMS spectra of reference Fe(II)-chukanovite CF0 after 2 months of ageing at RT: Measurements run at 77 K and 8 K. The experimental and computed curves are shown together with the various spectral components.

Figure 4: XRD patterns of CF0 precipitates after 15, 30 and 60 minutes of oxidation by air. The main diffraction peaks of chukanovite are denoted by the corresponding Miller index. Ghkl lines are those of goethite.

Figure 5: FTIR spectrum of CF0 precipitate after 30 minutes of oxidation; the vibration bands of chukanovite are denoted by their location in cm^{-1}.

Figure 6: TMS spectra run at RT and 77 K of CF0 precipitate after 30 minutes of oxidation by air. The experimental and computed curves are shown together with the various spectral components.

Figure 7: XRD patterns of CF0 precipitates after 15 minutes and 30 minutes of oxidation by air followed by 8 months of ageing at RT: Whole pattern of the precipitate oxidized 15 minutes (a) and detailed view of the 32°-46° angular region of the patterns of the precipitates oxidized 15 and 30 minutes. The main diffraction peaks of chukanovite are denoted by the corresponding Miller index. Mhkl and Ghkl lines are those of magnetite and goethite respectively.

Figure 8: Rietveld analysis of the XRD data obtained for CF0 precipitate after (a) 15 minutes or (b) 60 minutes of oxidation by air followed by 10 months of ageing. Experimental pattern (black dots), computed pattern (light grey line), error curve (black dotted line) and contributions of chukanovite (grey dash line), and magnetite (black line).

Figure 9: XRD pattern of CF0 precipitate after 15 minutes of oxidation by air followed by 15 minutes, 7 days or 10 months of ageing at RT. Mhkl lines are those of magnetite whereas the other, unindexed, diffraction peaks are those of chukanovite.

Figure 10: Raman spectra of CF0 precipitate after 2 weeks of ageing at RT (a) and CF0 precipitate after 60 minutes of oxidation by air followed by 1 month of ageing at RT (b). A letter and their position in cm^{-1} denote the vibration bands. Ck = chukanovite, G = goethite and M = magnetite.

Figure 11: XRD patterns of the precipitates obtained by coprecipitation of Fe(II) and Fe(III) salts. Whole pattern of the precipitate obtained with 5% Fe(III) (a) and detailed view of the 5°-35° angular region of the patterns of the precipitate obtained with 2%, 5% and 10% Fe(III).

The main diffraction peaks of chukanovite are denoted by the corresponding Miller index. GRhkl lines are those of sulfated green rust.

TABLES

Table 1. Hyperfine parameters obtained for Fe(II)-chukanovite CF0 at 77 K and 8 K. The error was determined by analyzing three samples. It was estimated at ±0.02 mm/s for CS and Δ in any case.

Sites	CS (mms^{-1})	Δ or ε (mms^{-1})	H (kOe)	Relative abundance (%)
77 K				
Fe1	1.23	2.56	-	52±4
Fe2	1.25	2.09	-	48±4
8 K				
Fe1	0.99	4.8	105	51±4
Fe2	1.31	3.8	240	46±4

Table 2. Lattice parameters of CF0 chukanovite precipitates with and without oxidation in air. The error was estimated via the analysis of two XRD patterns of each sample. The values given for χ^2 and R_{wp} are those of the best fit.

Sample	a (Å)	b (Å)	c (Å)	β (degree)	χ^2	R_{wp} (%)
CF0	12.35±0.02	9.37±0.01	3.200±0.005	97.04±0.08	1.09	1.85
CF0 + 15’ ox.	12.42±0.02	9.31±0.02	3.190±0.005	96.5±0.5	1.08	1.64
CF0 + 30’ ox.	12.47±0.02	9.28±0.02	3.200±0.005	96.0±0.1	1.25	1.96
CF0 + 60’ ox.	12.56±0.03	9.16±0.03	3.205±0.005	95.1±0.1	1.10	1.75

Table 3. Hyperfine parameters (RT) obtained for chukanovite CF0 oxidized 30 minutes The error was determined by analyzing three samples. It was estimated at ±0.02 mm/s for CS and Δ in any case.

Sites	CS (mms^{-1})	Δ (mms^{-1})	Relative abundance (%)
RT			
Fe1	1.16	2.58	47(±5)
Fe2	1.13	1.99	42(±4)
Doublet Fe(III)	0.32	0.87	11(±1)
77 K			
Fe1	1.25	2.58	45(±4)
Fe2	1.25	2.06	42(±4)
Doublet Fe(III)	0.73	0.74	13(±1)

Table 4. Lattice parameters of chukanovite and phase composition (wt.%) of oxidized samples of chukanovite CF0 after 9-10 months of ageing. Ck = chukanovite, M = magnetite and G = goethite. The error was estimated via the analysis of two XRD patterns of each sample. The values given for χ^2 and R_{wp} are those of the best fit.

Ox. time	a (Å)	b (Å)	c (Å)	β (degree)	%Ck	%M	%G	χ^2	R_{wp} (%)
15’	12.28±0.01	9.34±0.01	3.197±0.003	98.1±0.4	98±1	2±1	0	1.3	1.8
30’	12.30±0.03	9.33±0.03	3.196±0.001	97.87±0.01	95±1	5±1	0	1.1	3.5
60’	12.35±0.02	9.30±0.02	3.196±0.02	97.88±0.05	79±4	12±2	9±2	1.6	2.6

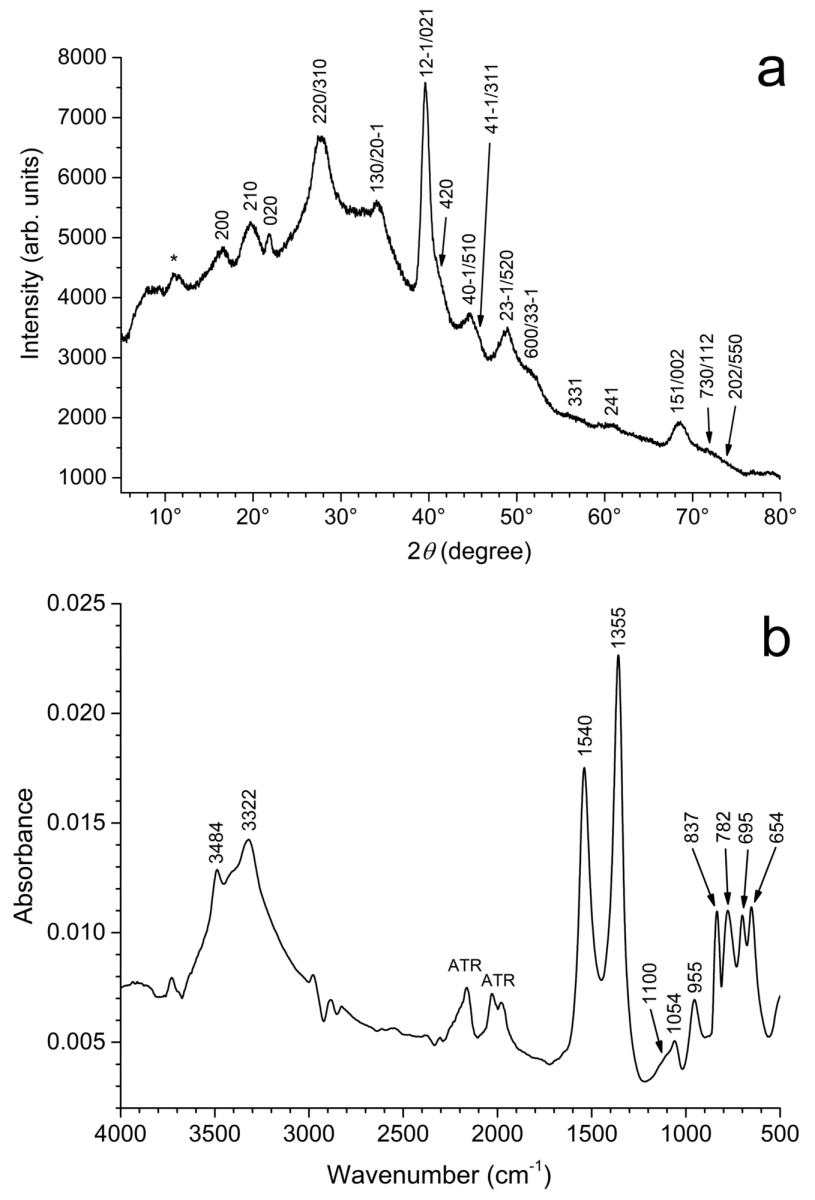
a
Intensity (arb. units)
2θ (degree)
*
200
210
020
220/310
130/20-1
12-1/021
420
41-1/311
40-1/510
23-1/520
600/33-1
331
241
151/002
730/112
202/550
b
Absorbance
Wavenumber (cm-1)
3484
3322
ATR
ATR
1540
1355
1100
1054
955
837
782
695
654

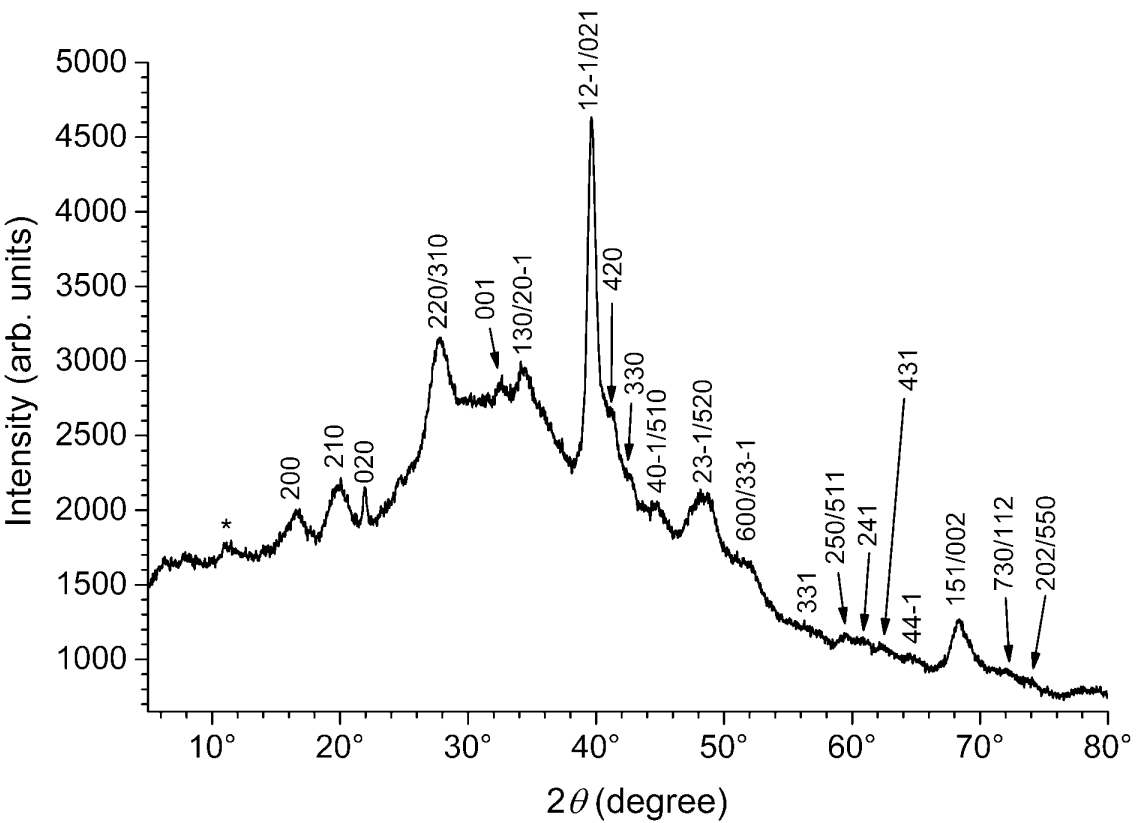
Intensity (arb. units)
5000
4500
4000
3500
3000
2500
2000
1500
1000
10°
20°
30°
40°
50°
60°
70°
80°
2θ (degree)
*
200
210
020
220/310
001
130/20-1
12-1/021
420
330
40-1/510
23-1/520
600/33-1
331
250/511
241
431
44-1
151/002
730/112
202/550

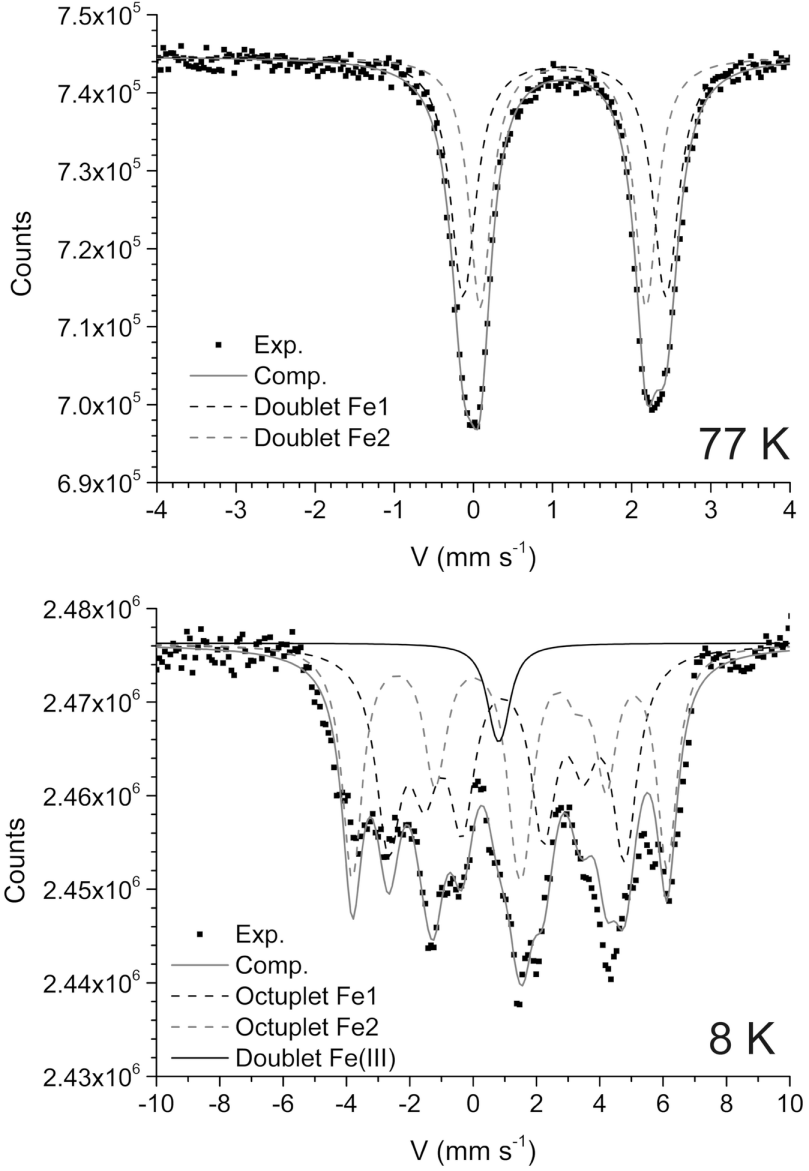
7.5x10^5
7.4x10^5
7.3x10^5
7.2x10^5
7.1x10^5
7.0x10^5
6.9x10^5
Counts
Exp.
Comp.
Doublet Fe1
Doublet Fe2
77 K
-4
-3
-2
-1
0
1
2
3
4
V (mm s^-1)
2.48x10^6
2.47x10^6
2.46x10^6
2.45x10^6
2.44x10^6
2.43x10^6
Counts
Exp.
Comp.
Octuplet Fe1
Octuplet Fe2
Doublet Fe(III)
8 K
-10
-8
-6
-4
-2
0
2
4
6
8
10
V (mm s^-1)

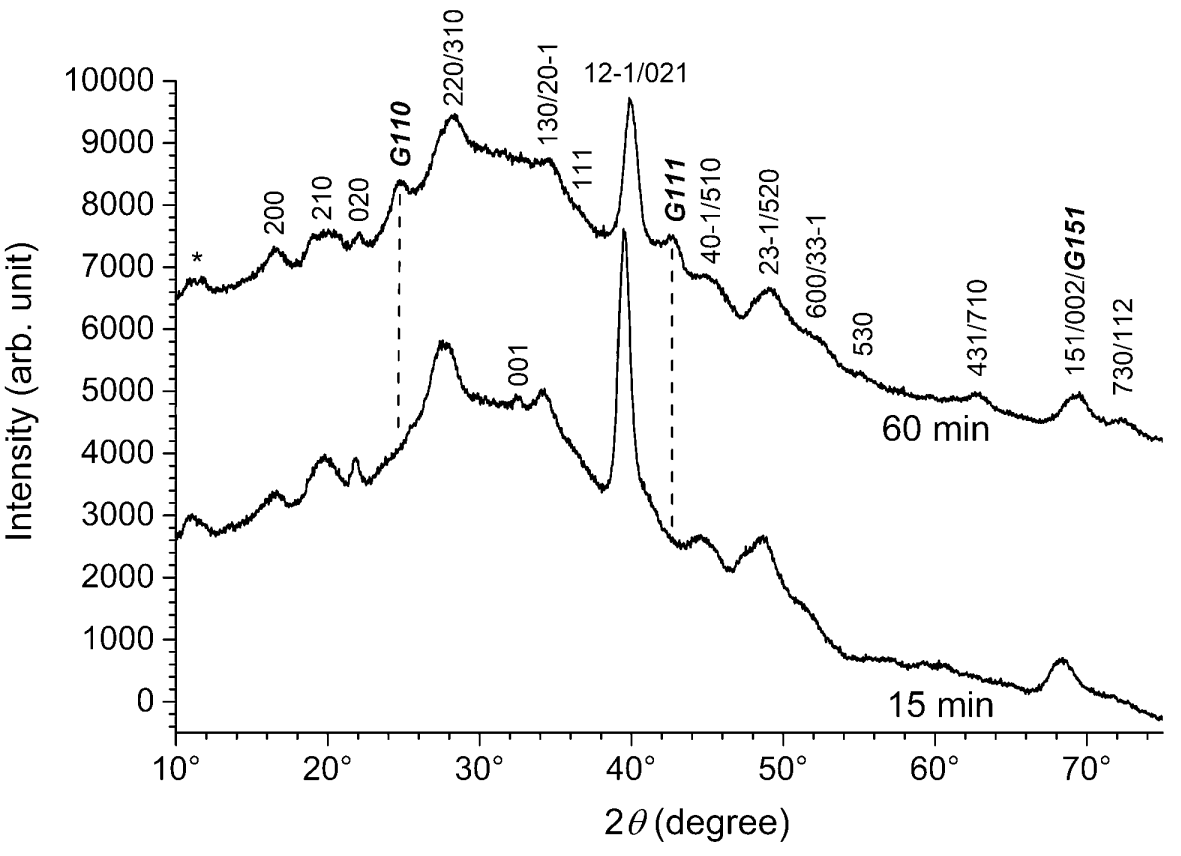
Intensity (arb. unit)
10000
9000
8000
7000
6000
5000
4000
3000
2000
1000
0
10°
20°
30°
40°
50°
60°
70°
2θ (degree)
*
200
210
020
G110
220/310
130/20-1
111
12-1/021
G111
40-1/510
23-1/520
600/33-1
530
431/710
151/002/G151
730/112
60 min
001
15 min

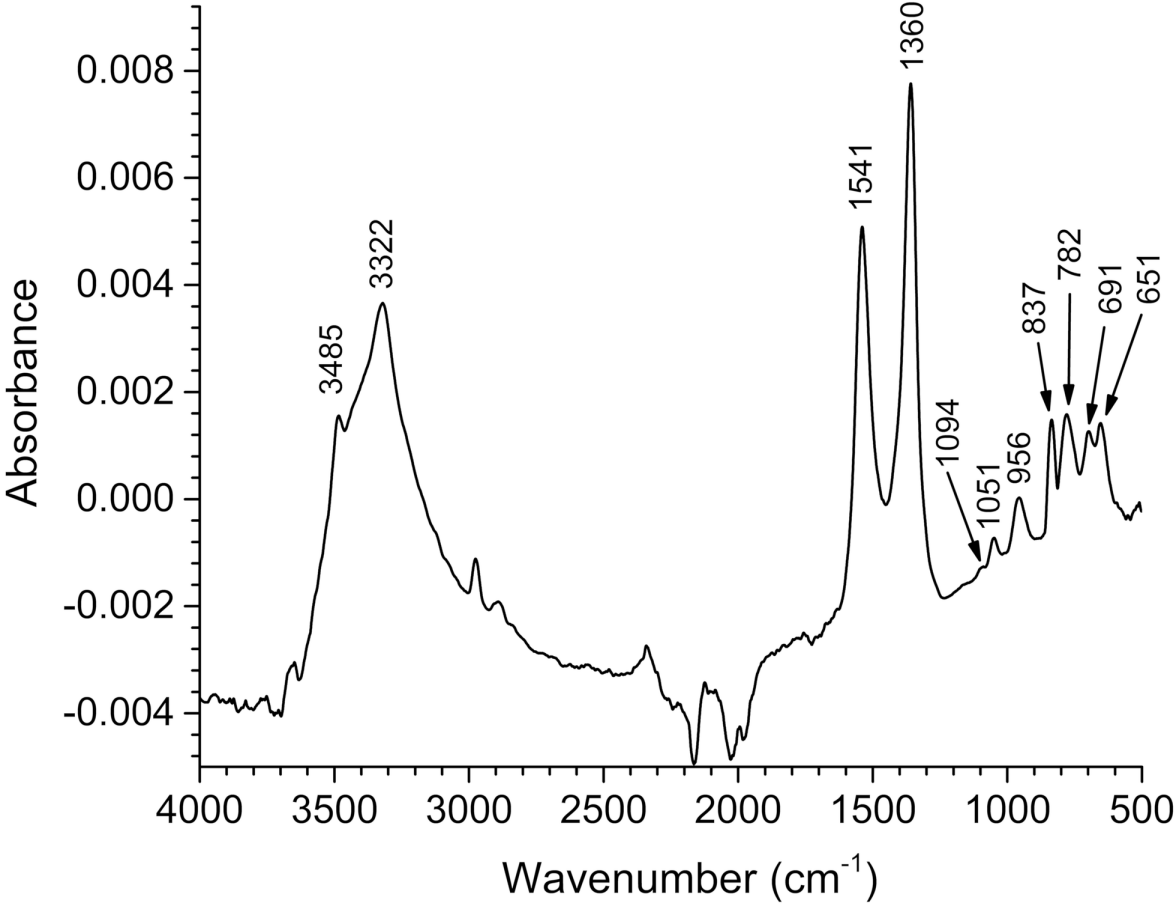
0.008
0.006
0.004
0.002
0.000
-0.002
-0.004
Absorbance
4000
3500
3000
2500
2000
1500
1000
500
Wavenumber (cm-1)
3485
3322
1541
1360
1094
1051
956
837
782
691
651

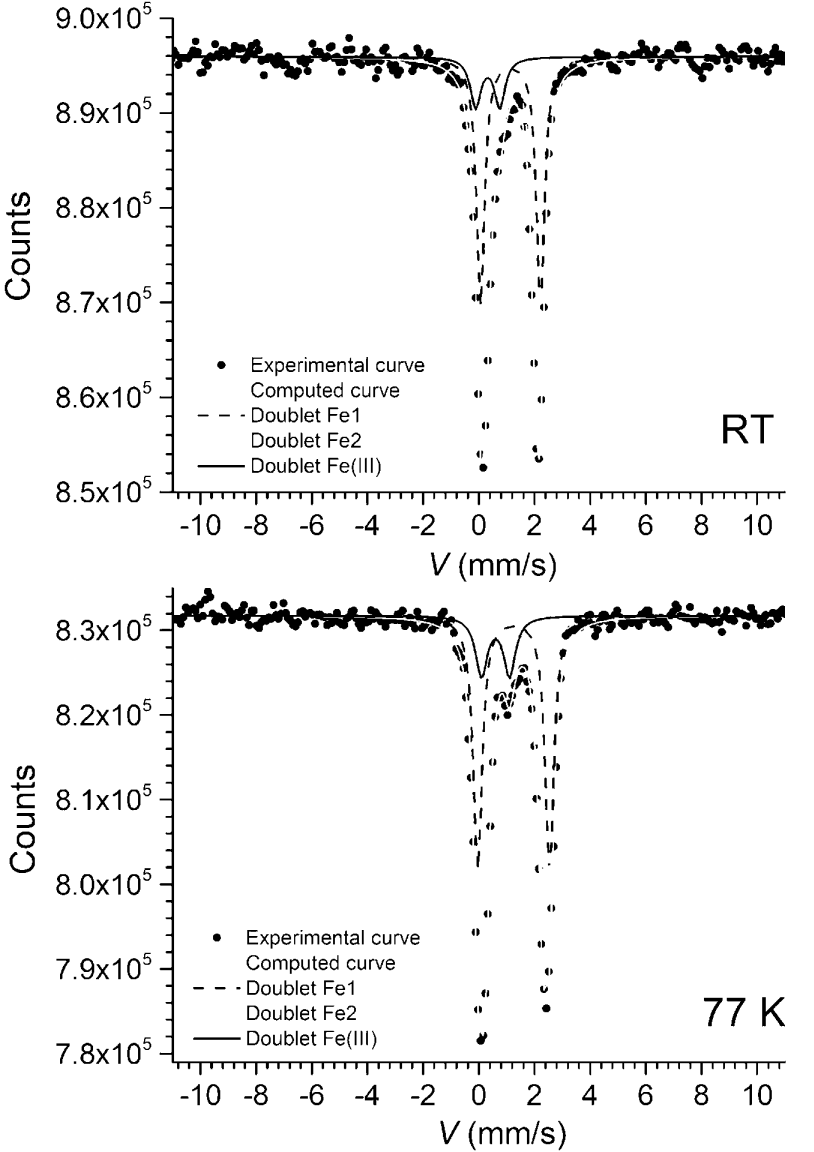
9.0x10^5
8.9x10^5
8.8x10^5
8.7x10^5
8.6x10^5
8.5x10^5
Counts
Experimental curve
Computed curve
Doublet Fe1
Doublet Fe2
Doublet Fe(III)
RT
-10 -8 -6 -4 -2 0 2 4 6 8 10
V (mm/s)
8.3x10^5
8.2x10^5
8.1x10^5
8.0x10^5
7.9x10^5
7.8x10^5
Counts
Experimental curve
Computed curve
Doublet Fe1
Doublet Fe2
Doublet Fe(III)
77 K
-10 -8 -6 -4 -2 0 2 4 6 8 10
V (mm/s)

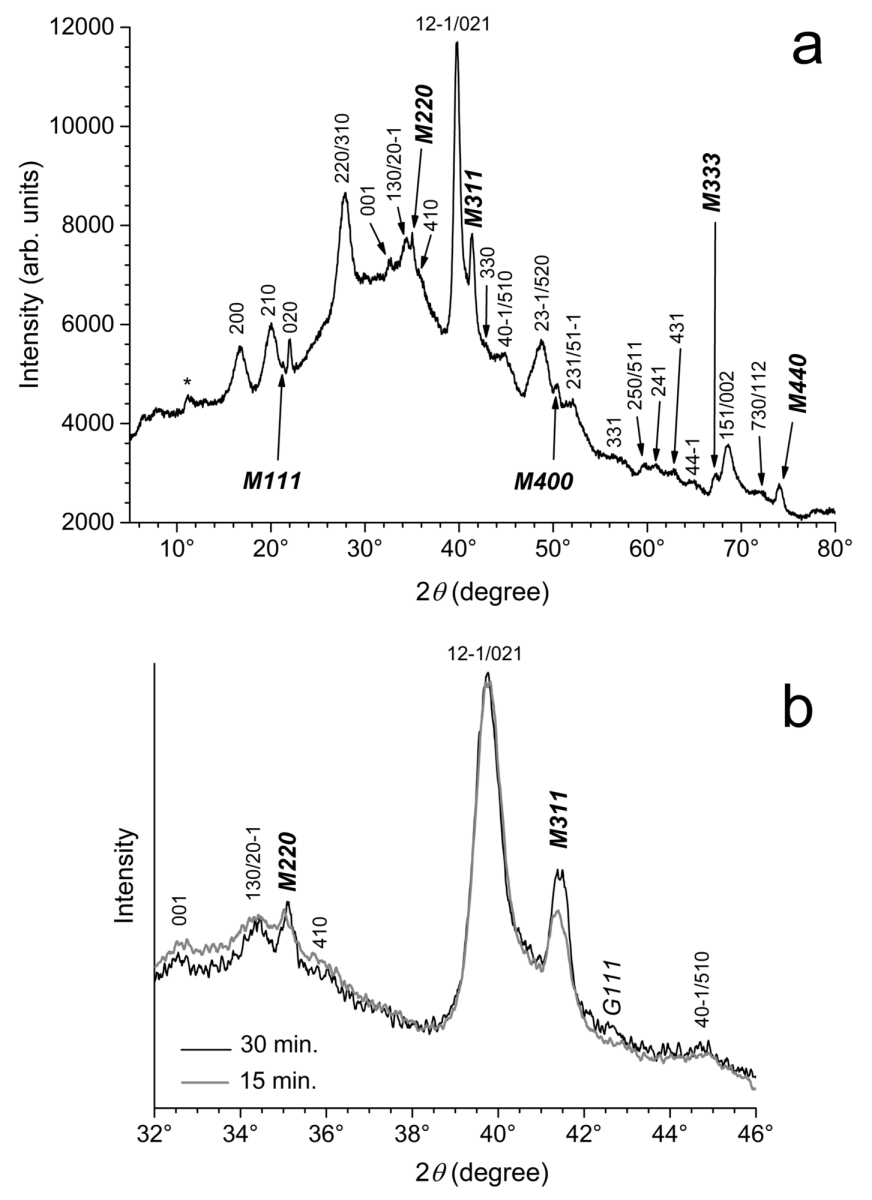
a
Intensity (arb. units)
2θ (degree)
12-1/021
220/310
001
130/20-1
M220
410
M311
330
40-1/510
23-1/520
231/51-1
M333
331
250/511
241
431
44-1
151/002
730/112
M440
200
210
020
*
M111
M400
b
Intensity
001
130/20-1
M220
410
12-1/021
M311
G111
40-1/510
30 min.
15 min.
2θ (degree)

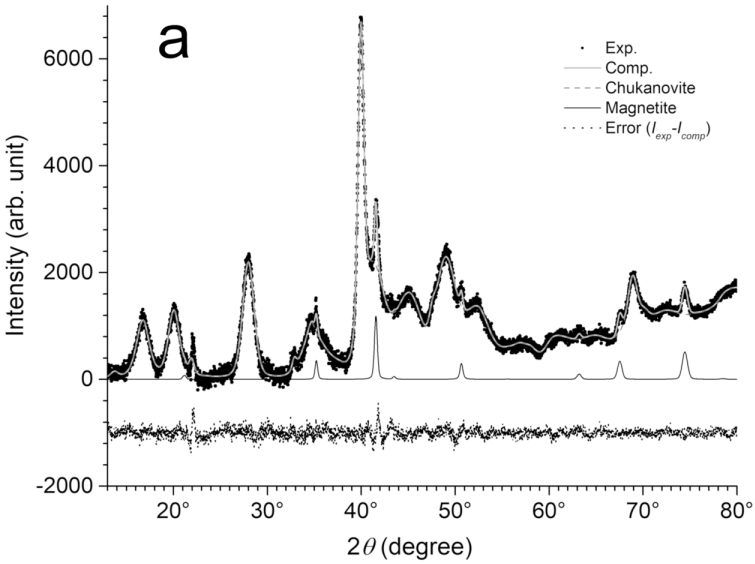
a
Exp.
Comp.
Chukanovite
Magnetite
Error (I_{exp}-I_{comp})
Intensity (arb. unit)
6000
4000
2000
0
-2000
20°
30°
40°
50°
60°
70°
80°
2θ (degree)

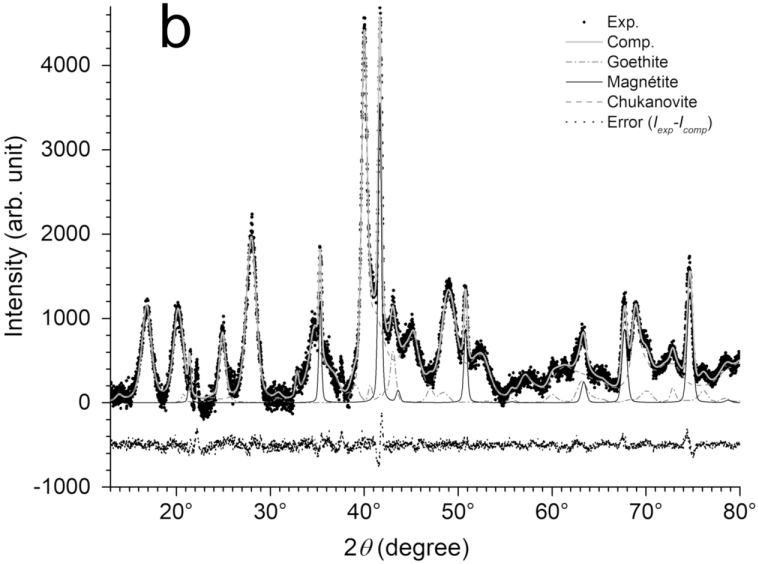
b
Exp.
Comp.
Goethite
Magnétite
Chukanovite
Error (I_{exp}-I_{comp})
Intensity (arb. unit)
4000
3000
2000
1000
0
-1000
20°
30°
40°
50°
60°
70°
80°
2θ (degree)

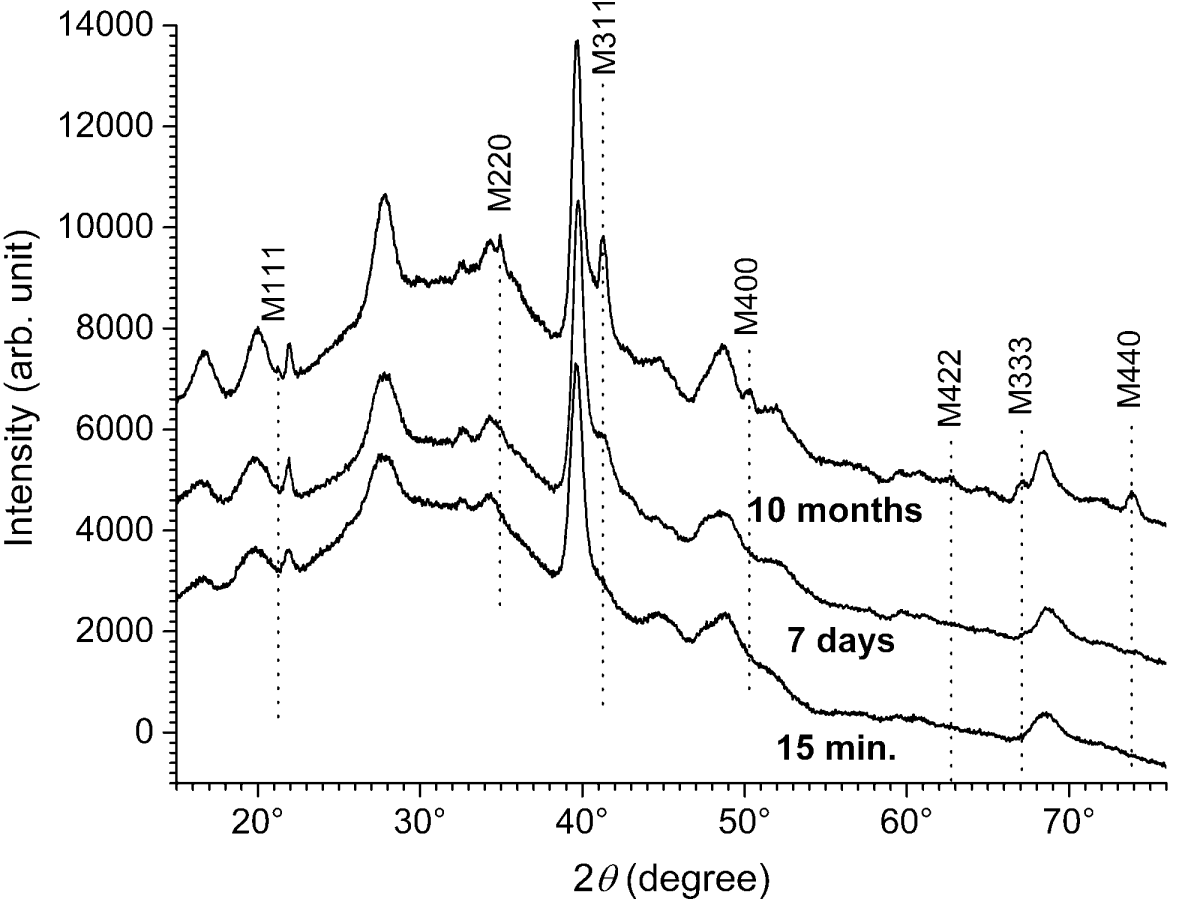
14000
12000
10000
8000
6000
4000
2000
0
Intensity (arb. unit)
M111
M220
M311
M400
M422
M333
M440
10 months
7 days
15 min.
20°
30°
40°
50°
60°
70°
2θ (degree)

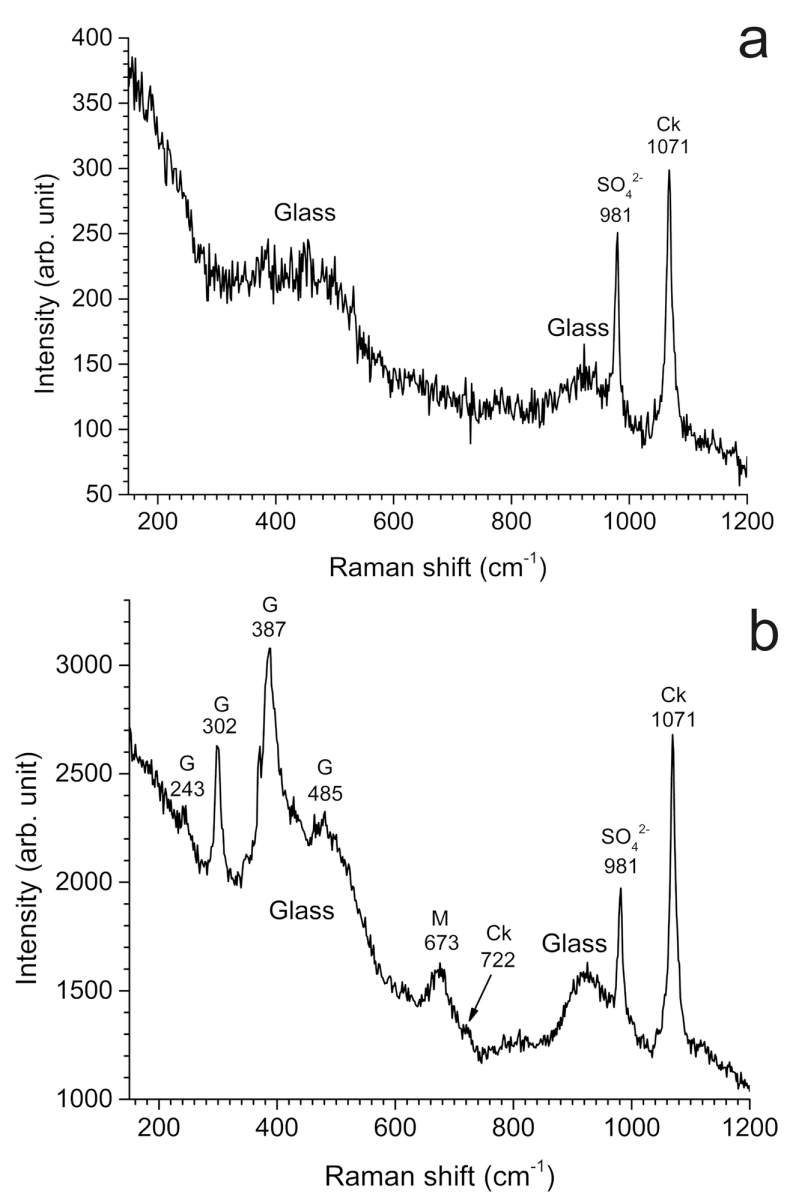
a
Intensity (arb. unit)
Raman shift (cm-1)
Glass
Glass
SO4 2-
981
Ck
1071
b
Intensity (arb. unit)
Raman shift (cm-1)
G
243
G
302
G
387
G
485
Glass
M
673
Ck
722
Glass
SO4 2-
981
Ck
1071

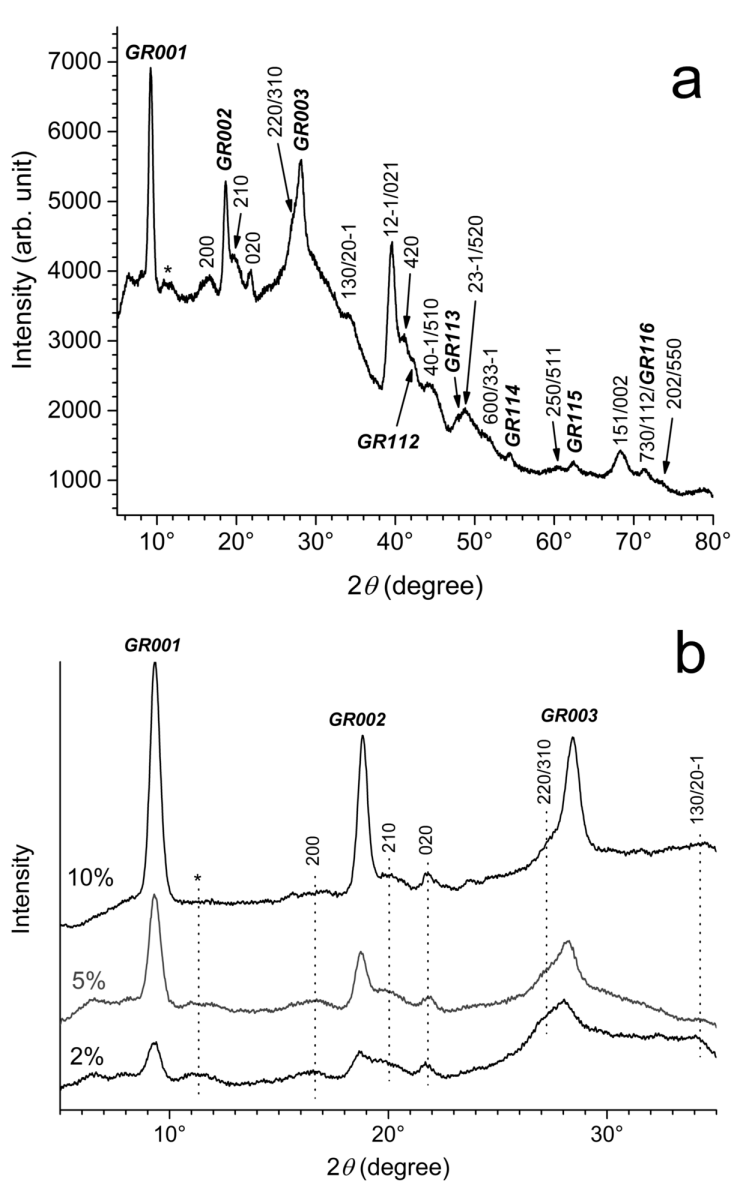
a
Intensity (arb. unit)
2θ (degree)
GR001
GR002
GR003
GR112
GR113
GR114
GR115
GR116
200
210
020
220/310
130/20-1
12-1/021
420
40-1/510
23-1/520
600/33-1
250/511
151/002
730/112/
202/550
*
b
Intensity
2θ (degree)
10%
5%
2%
GR001
GR002
GR003
200
210
020
220/310
130/20-1
*

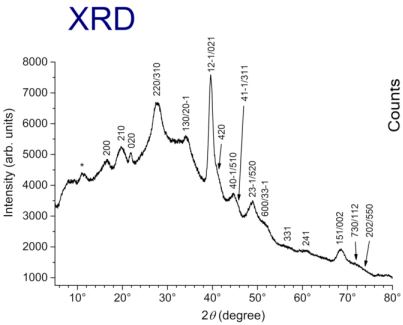

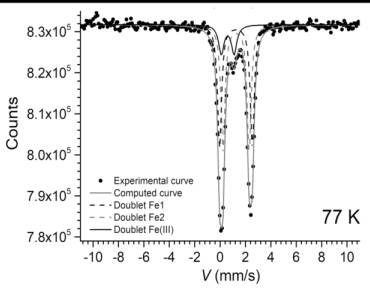

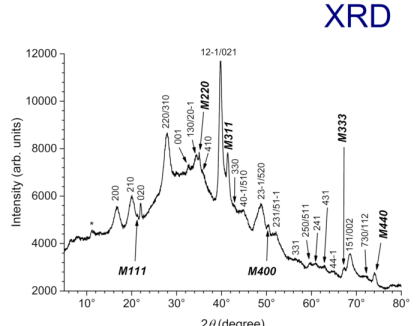

$Fe^{II}_{2-x}Fe^{III}_{x}(OH)_{2-x}O_xCO_3$ → Ageing 10 months in anoxic conditions → Fe(II)-chukanovite + magnetite